Global Ocean Tripole and Climate Variability

Peter C. Chu

Naval Postgraduate School

San Jose State University

Department of Meteorology and Climate Science

October 1, 2014

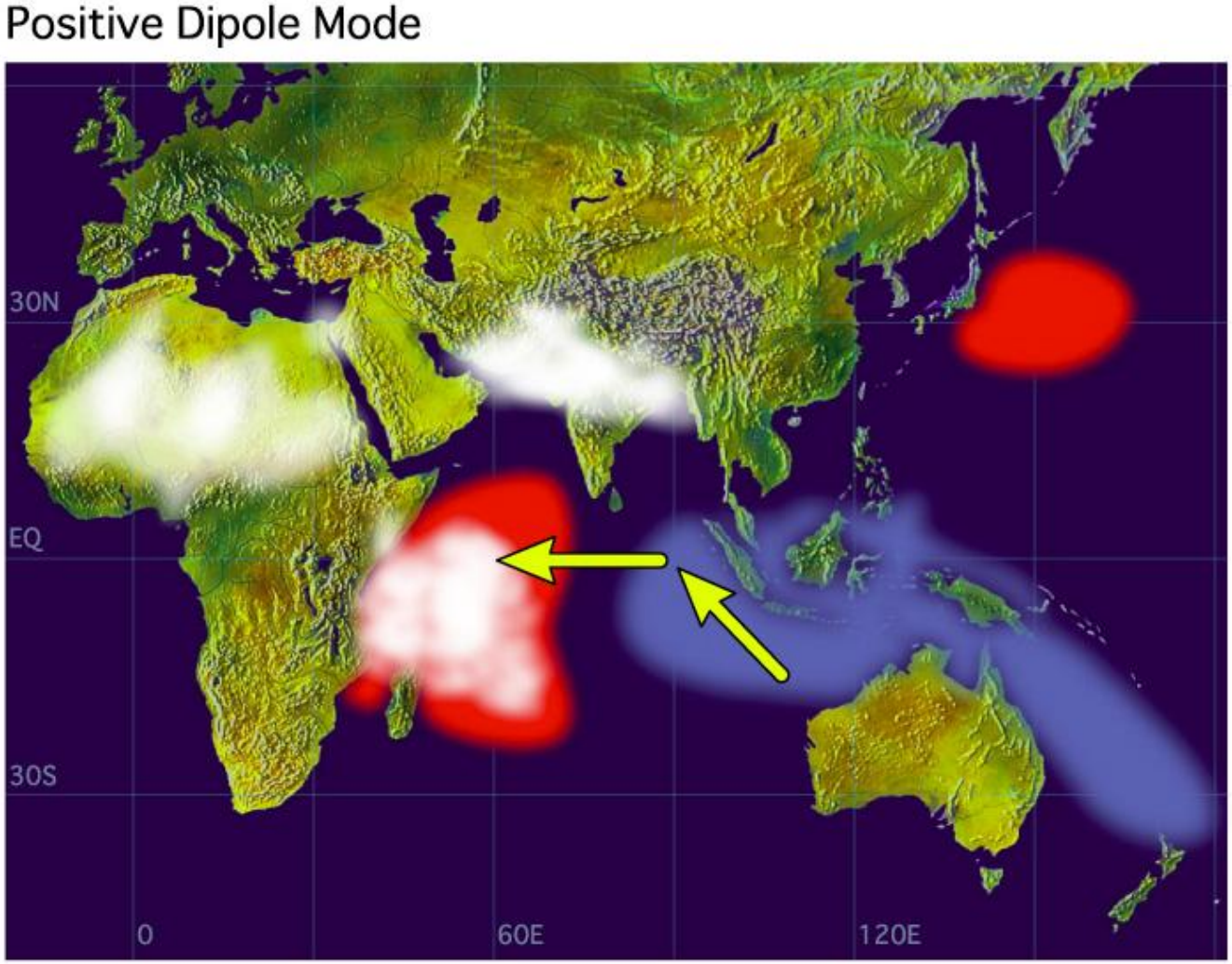
Outline

- (1) Recent Development in Short-term Climate Variability
- (2) Data Analysis: (T, S) Profiles → Synoptic Gridded Data with Monthly Increment
- (3) Synoptic Upper Ocean (0-300 m) Heat Content
- (4) Global Tripole → Canonical El Nino (East Pacific El Nino), El Nino Modoki (Central Pacific El Nino), Indian Ocean Dipole, …

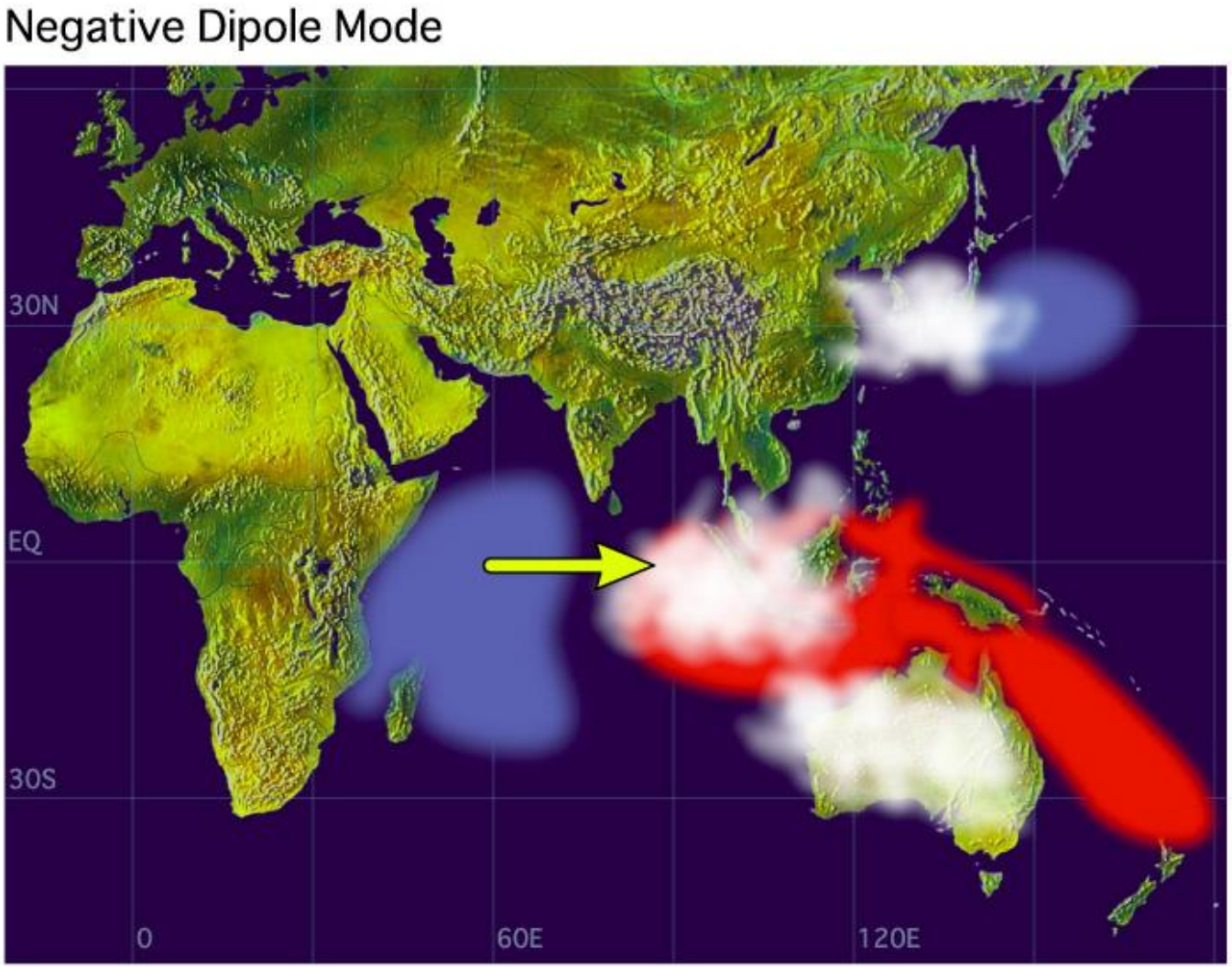
(1) Development in Climate Variability

Indian Ocean Dipole
Canonical (Eastern Pacific) El Nino
El Nino Modoki (Central Pacific El Nino)

Indian Ocean Dipole (Saji et al. 1999)



Indian Ocean Dipole (Saji et al. 1999)



Dipole Mode Index (DMI)

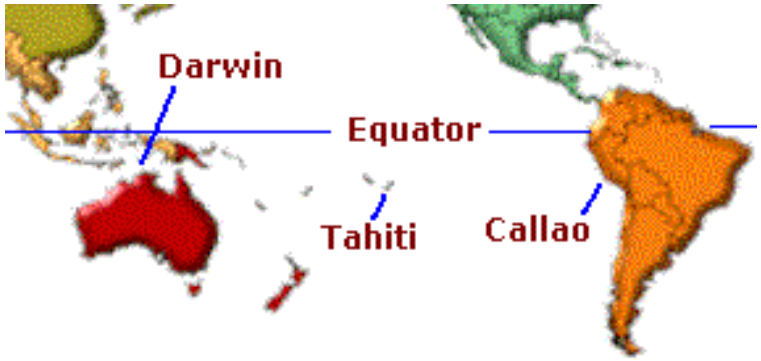
$$DMI = SSTA_{West} - SSTA_{East}$$

West = 50°E-70°E;10°S-10°N

East = 90°E-110°E;10° S-0°

Southern Oscillation Index (SOI)

$$s(\tilde{t}_p) = 10 \times \frac{p_{diff}(\tilde{t}_p) - \langle p_{diff} \rangle}{SD(p_{diff})}$$



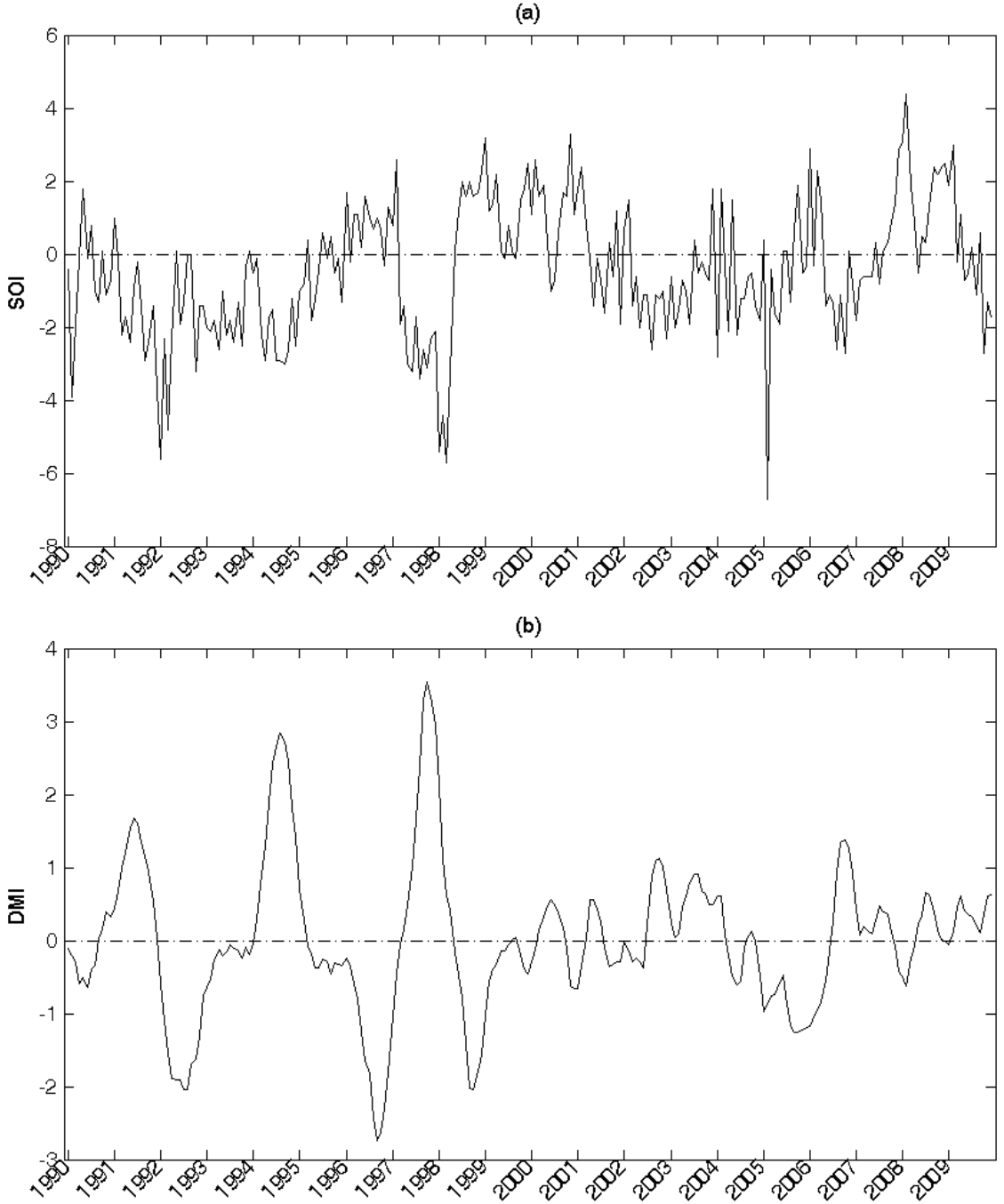
p_{diff} is the mean sea level pressure of Tahiti minus that of Darwin for that month;

$\langle p_{diff} \rangle$ is the long-term average of p_{diff} for the month

SD(p_{diff}) is the long-term standard deviation of p_{diff}

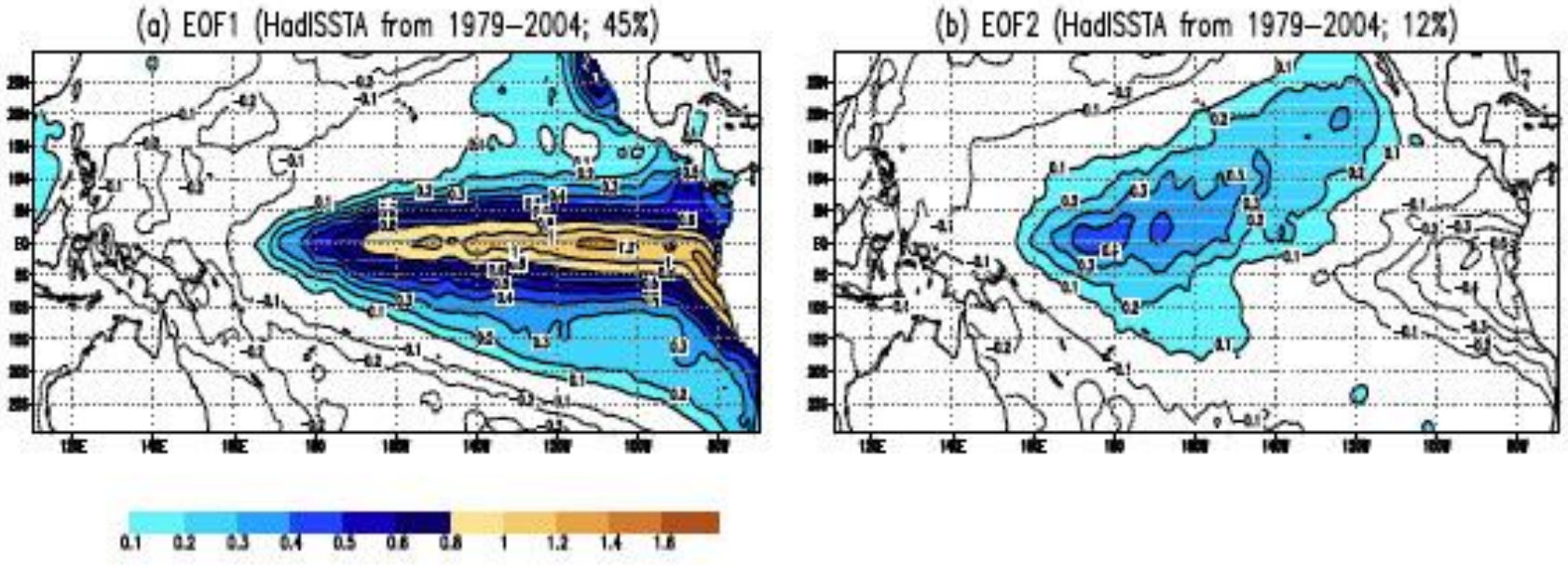
Southern Oscillation Index (SOI)

Dipole Mode Index (DMI)



El Nino and El Nino Modoki

(Weng et al. 2007, Ashok et al. 2007)



(Images from Karumuri Ashok, APEC Climate Center)

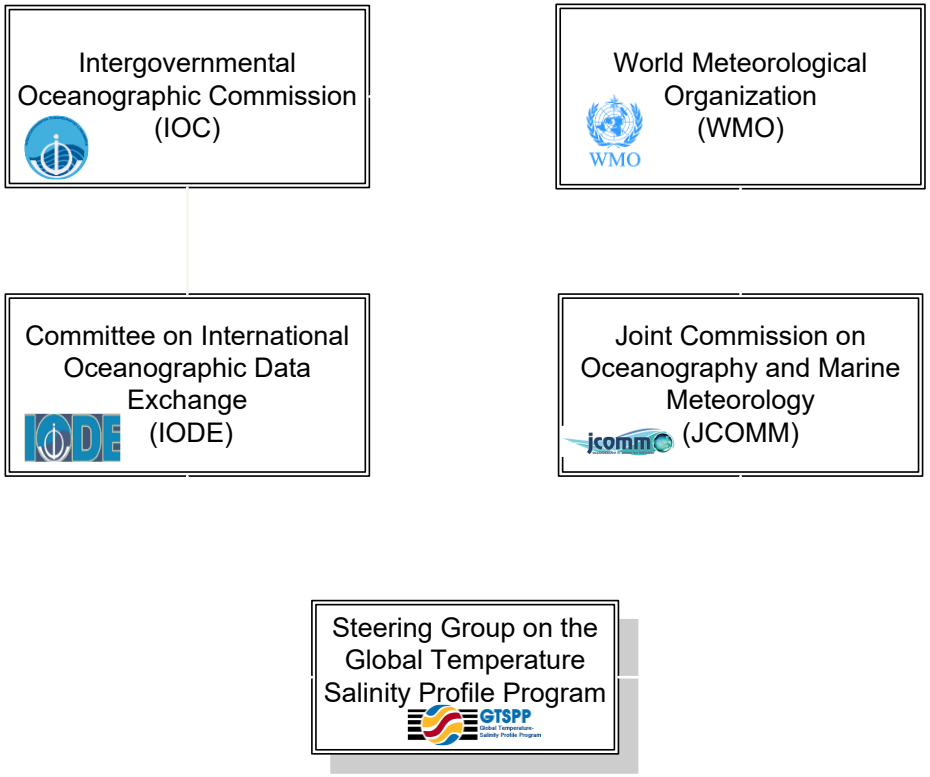
(2) Data Analysis

Global Temperature and Salinity Profile Program (GTSPP)

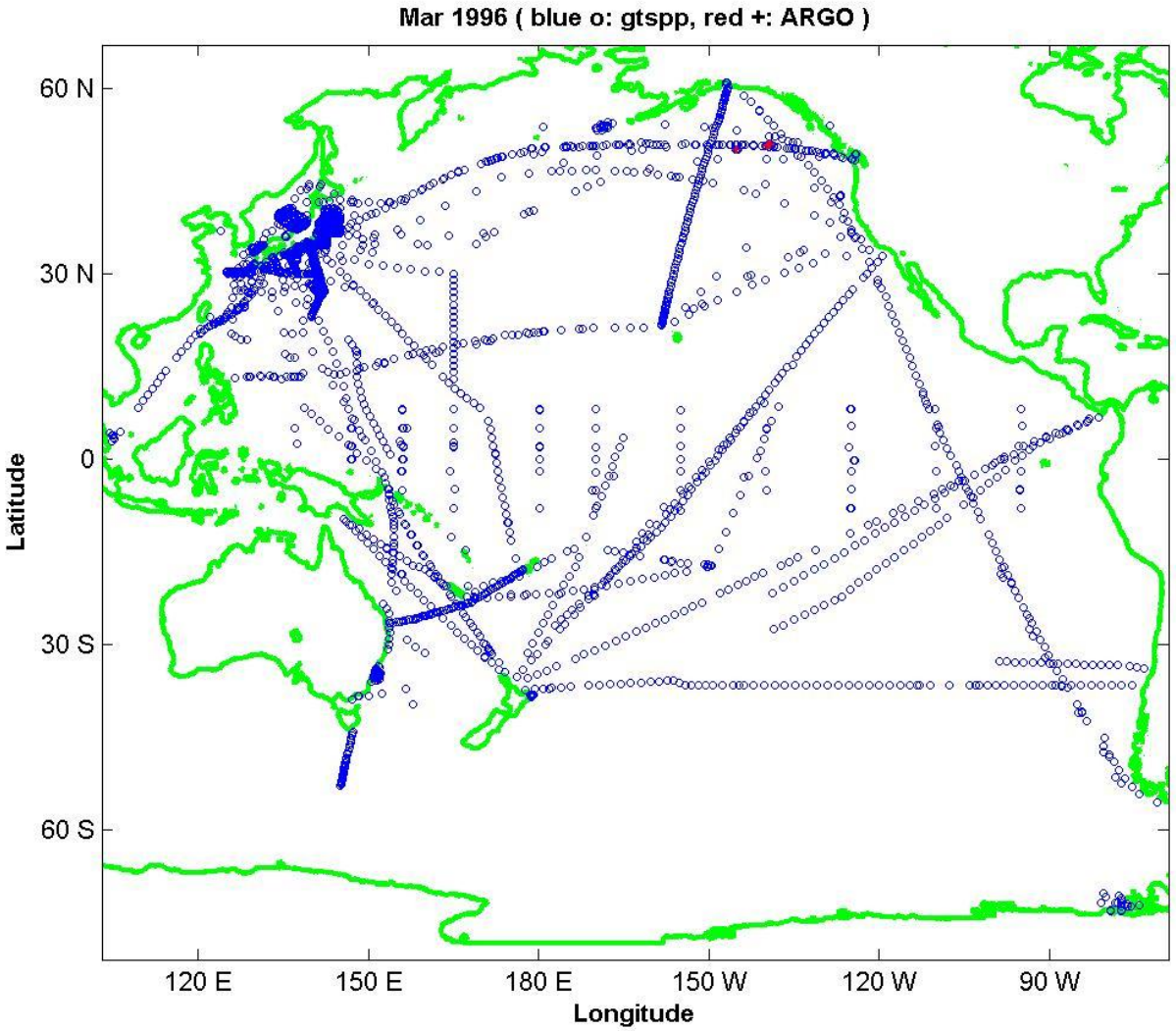
GTSPP

GTSPP = Global Temperature Salinity Profile Program

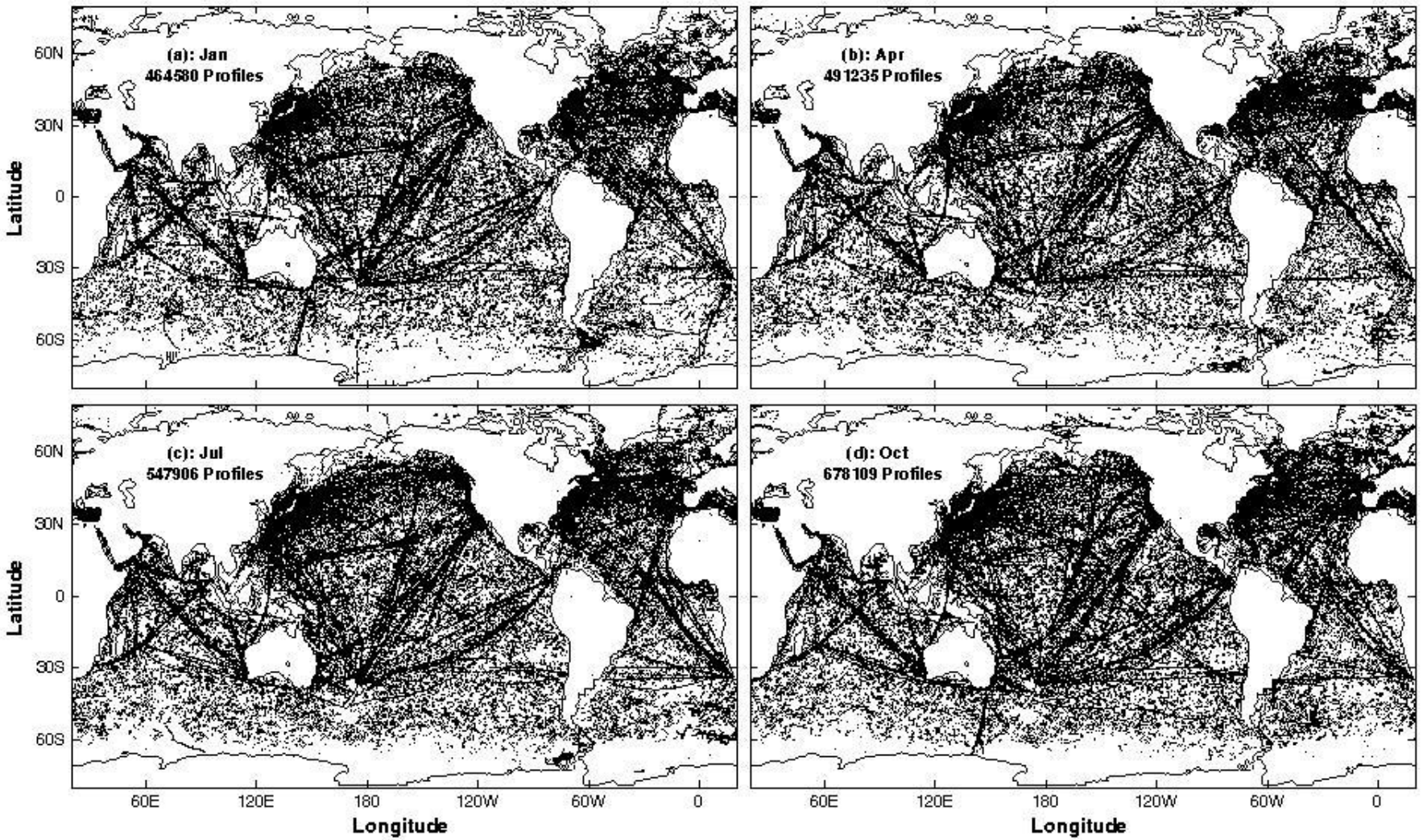
- GTSPP is a joint WMO-IOC program designed to provide improved access to the highest resolution, highest quality data as quickly as possible.
- GTSPP began as an official IODE pilot project in 1989.
- It went into operation in November 1990.



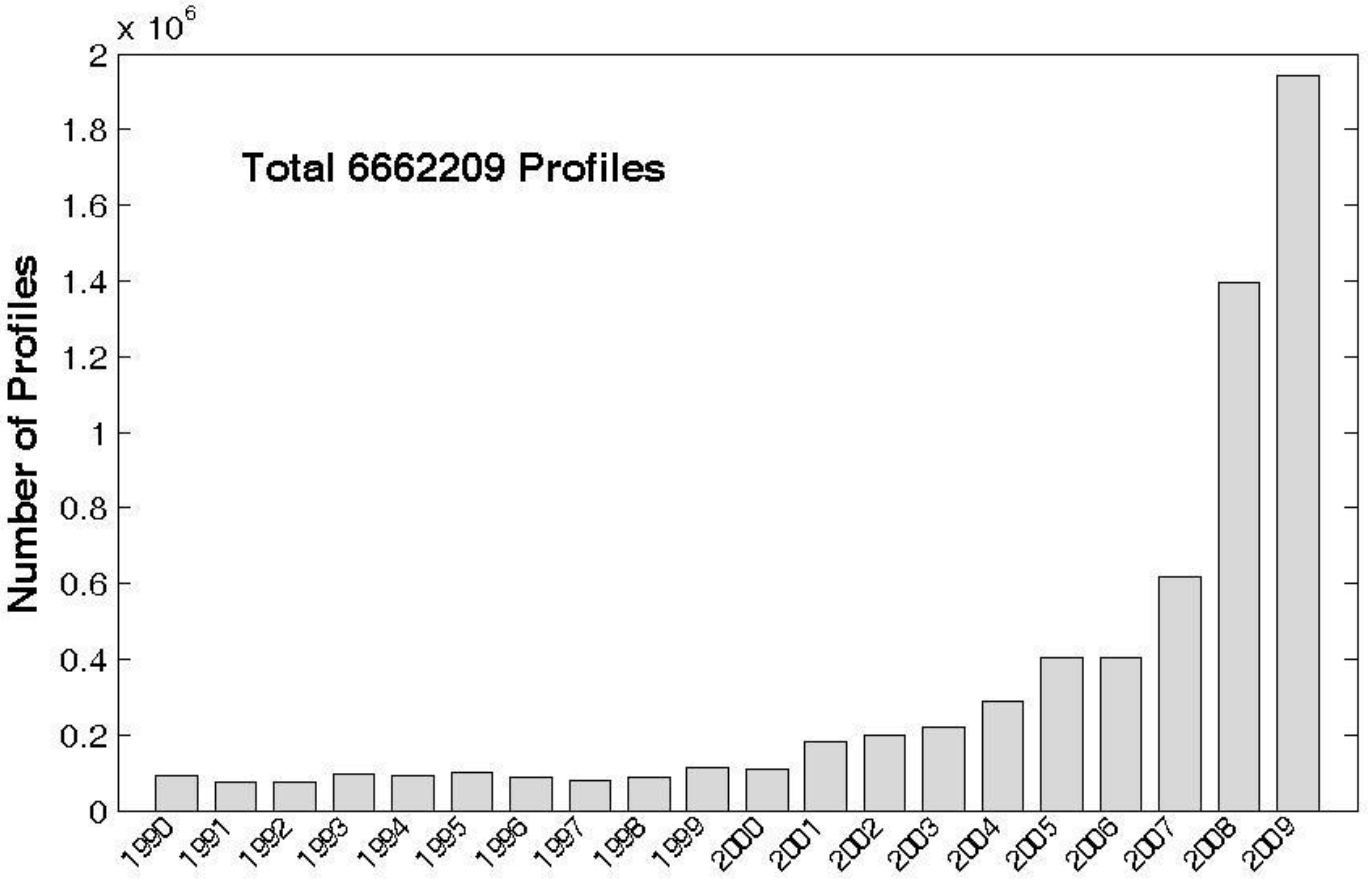
Example → GTSPP Data

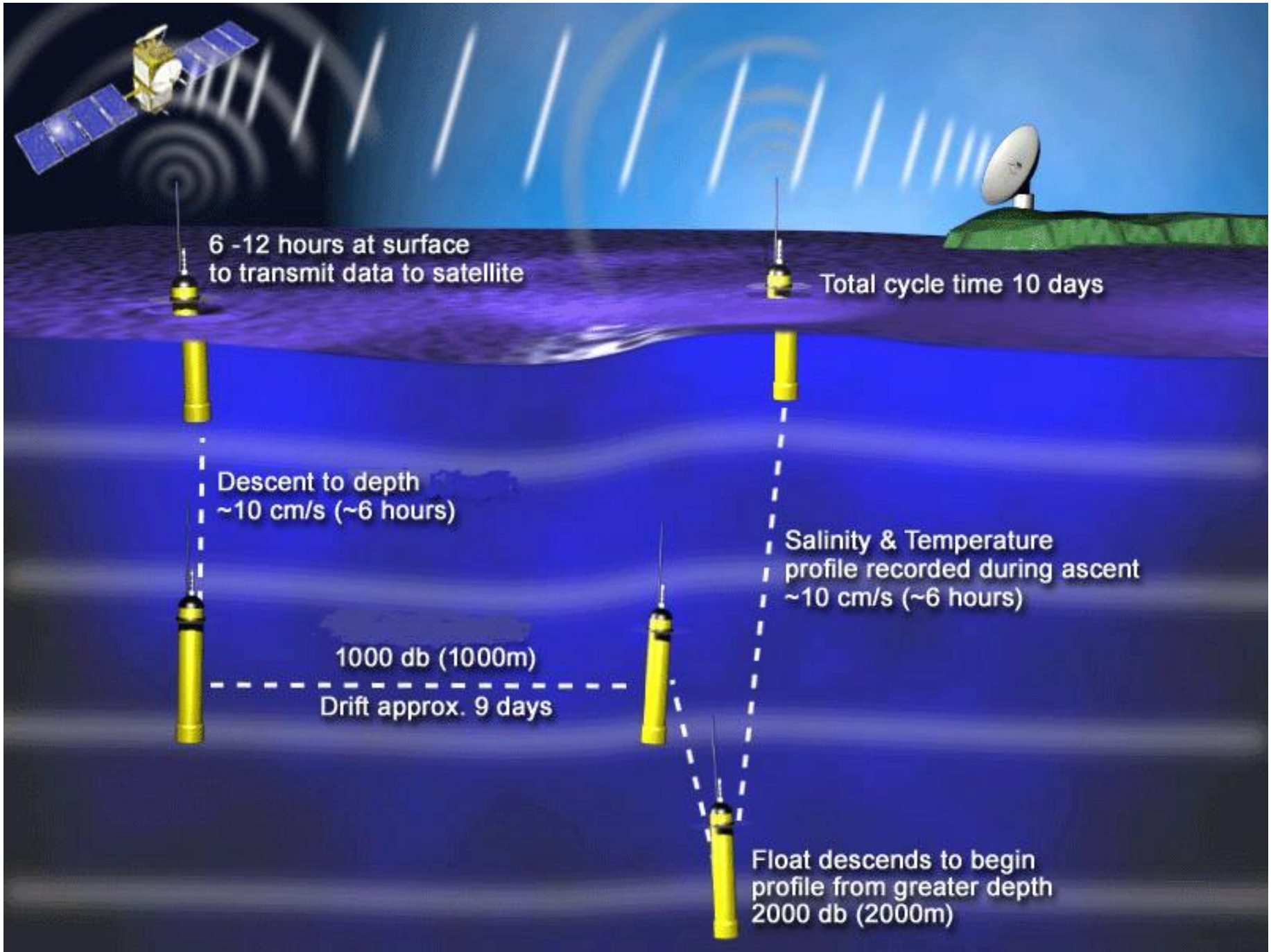


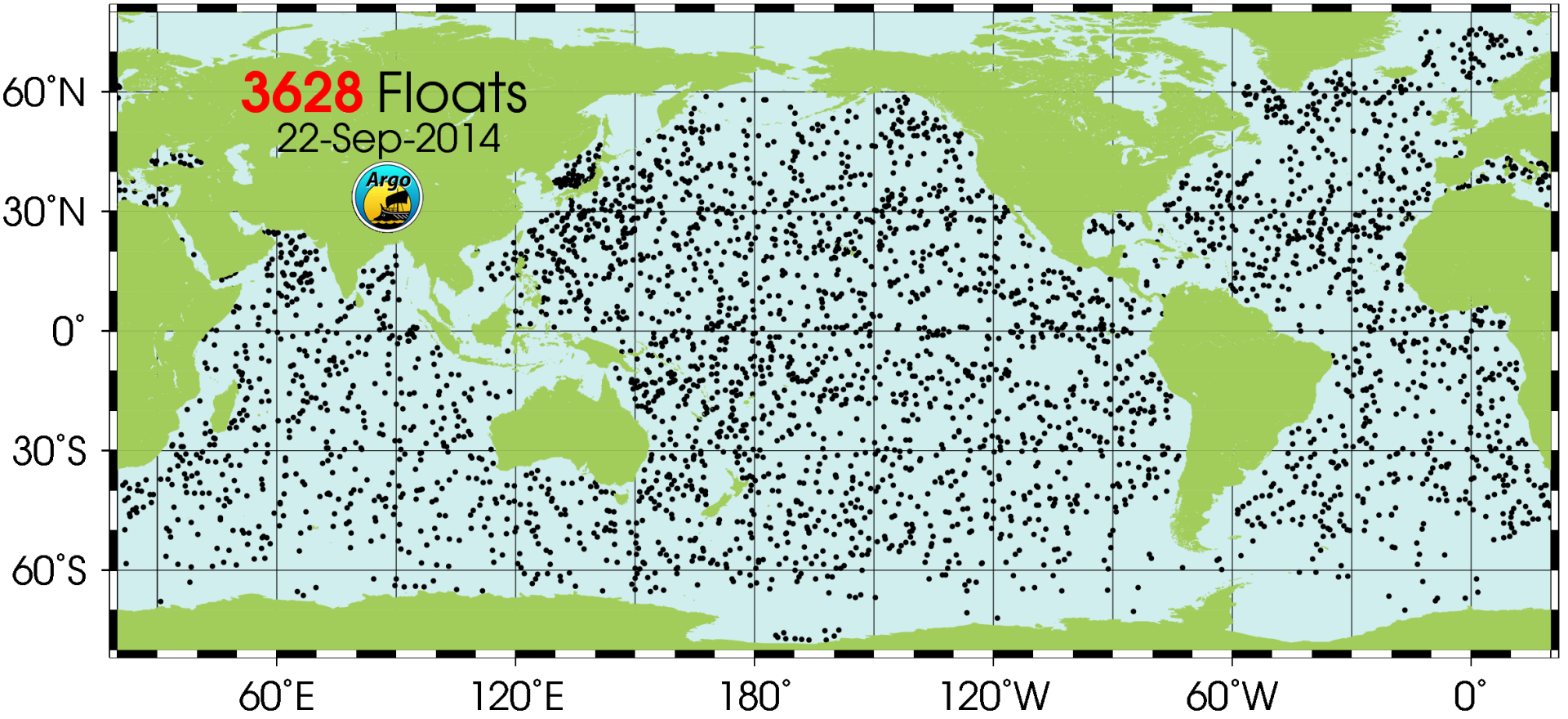
Spatial Distribution of GTSPP Data



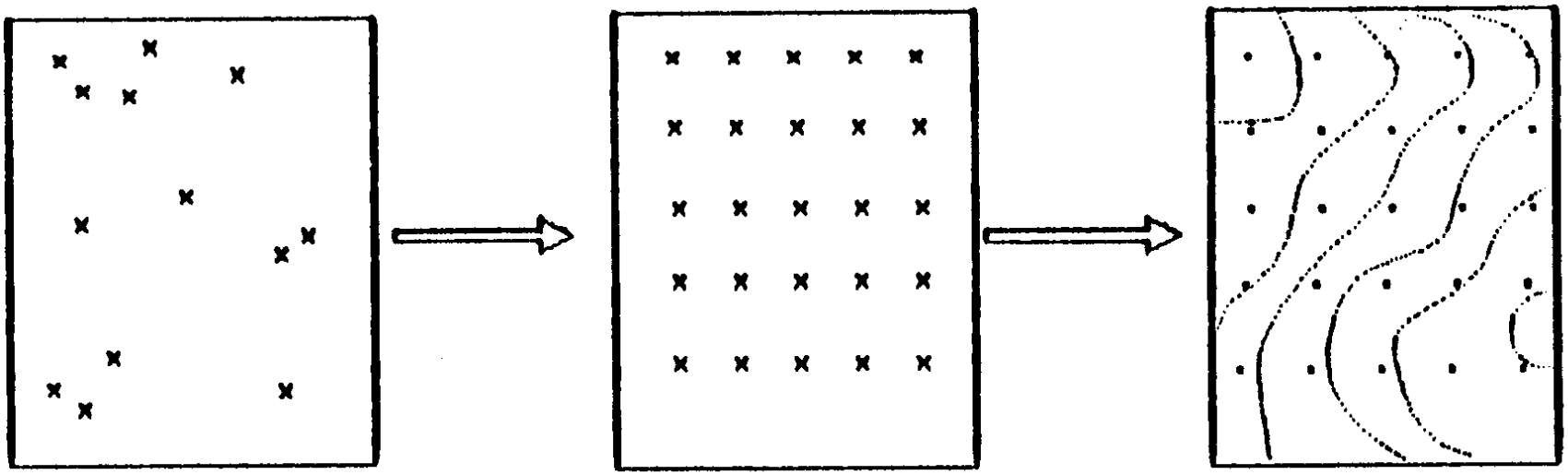
Temporal Distribution of GTSPP Data




6 -12 hours at surface
to transmit data to satellite
Total cycle time 10 days
Descent to depth
~10 cm/s (~6 hours)
Salinity & Temperature
profile recorded during ascent
~10 cm/s (~6 hours)
1000 db (1000m)
Drift approx. 9 days
Float descends to begin
profile from greater depth
2000 db (2000m)


3628 Floats
22-Sep-2014
Argo
60°N
30°N
0°
30°S
60°S
60°E
120°E
180°
120°W
60°W
0°

Ocean Data Analysis



Classical Method → Fourier Series Expansion

Joseph Fourier 1768-1830



Fourier was obsessed with the physics of heat and developed the Fourier series and transform to model heat-flow problems.

Fourier Series Expansion

For a rectangular region (L_x, L_y), the basis functions are sinusoidal functions.

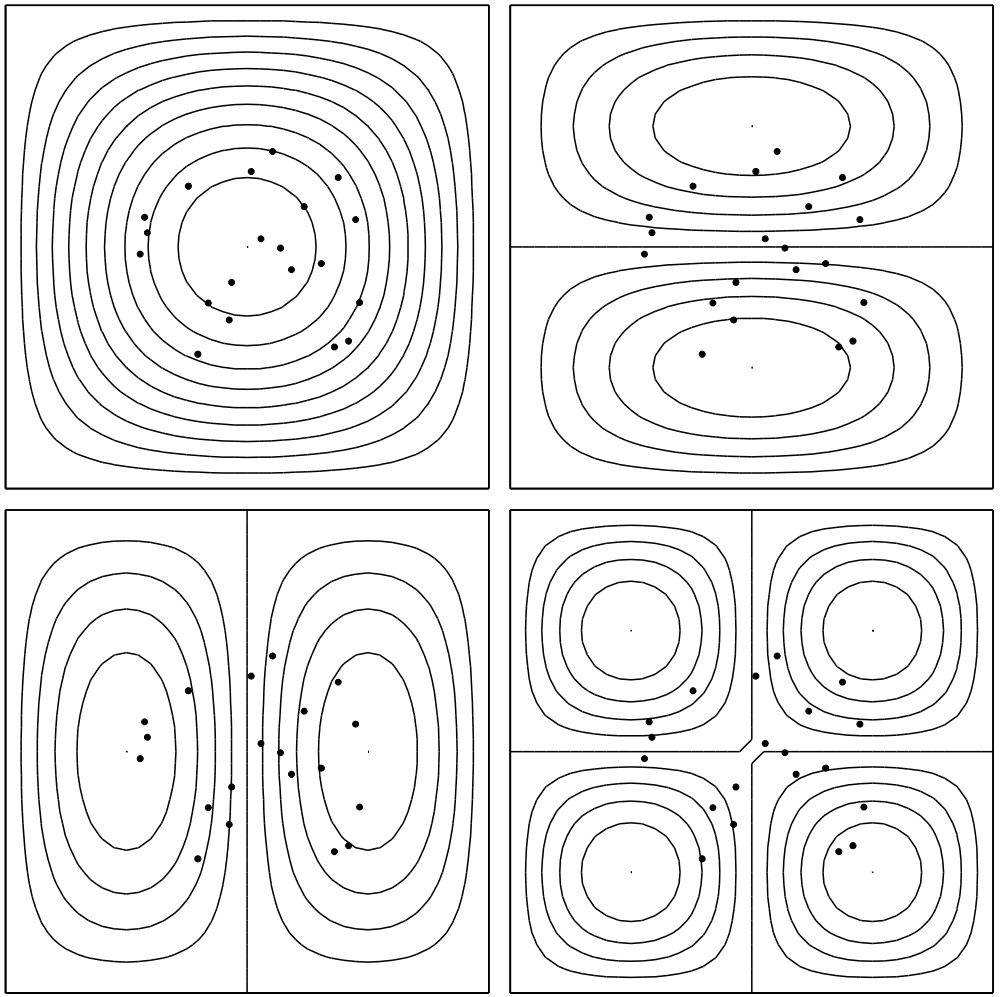
$$f(x,y) = \sum_i \sum_j a_{ij} \sin\frac{i\pi x}{L_x} \sin\frac{j\pi y}{L_y}$$

$$+\sum_i \sum_j b_{ij} \cos\frac{i\pi x}{L_x} \cos\frac{j\pi y}{L_y}$$

For the Dirichret boundary condition : $f = 0$ at the boundaries

$$f(x,y) = \sum_i \sum_j a_{ij} \sin\frac{i\pi x}{L_x} \sin\frac{j\pi y}{L_y}$$

The dots represent the Observations.



Linear Algebraic Equations for the Coefficients a_{ij}

$$f(x_1^{ob}, y_1^{ob}) = \sum_i \sum_j a_{ij} \sin \frac{i\pi x_1^{ob}}{L_x} \sin \frac{j\pi y_1^{ob}}{L_y}$$

$$f(x_2^{ob}, y_2^{ob}) = \sum_i \sum_j a_{ij} \sin \frac{i\pi x_2^{ob}}{L_x} \sin \frac{j\pi y_2^{ob}}{L_y}$$

.....

$$f(x_M^{ob}, y_M^{ob}) = \sum_i \sum_j a_{ij} \sin \frac{i\pi x_M^{ob}}{L_x} \sin \frac{j\pi y_M^{ob}}{L_y}$$

Determination of Spectral Coefficients (Ill-Posed Algebraic Equation)

$$\mathbf{A}\,\hat{\mathbf{a}} = \mathbf{Q}\mathbf{Y},$$

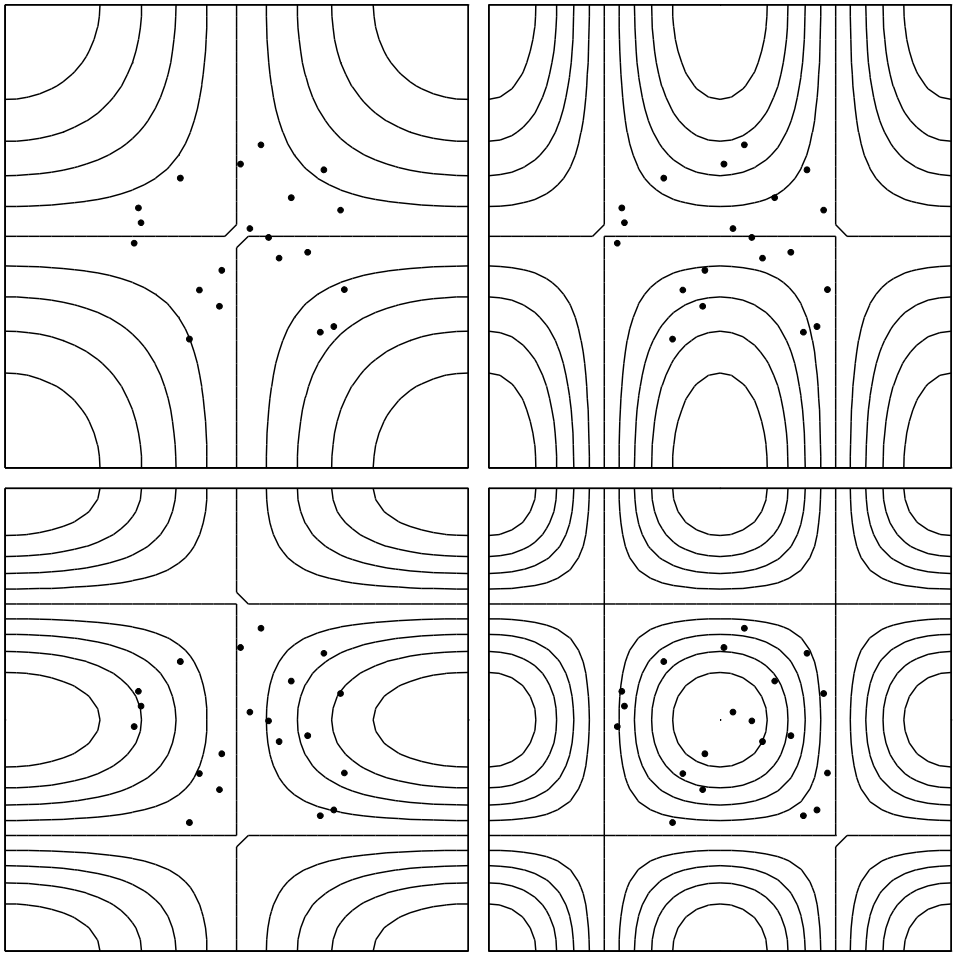
Known a_{ij} → Analyzed Field

$$f(x,y) = \sum_i \sum_j a_{ij} \sin \frac{i\pi x}{L_x} \sin \frac{j\pi y}{L_y}$$

For the Neumann boundary condition $n \bullet \nabla f = 0$ at the boundaries

$$f(x,y) = \sum_i \sum_j b_{ij} \cos \frac{i\pi x}{L_x} \cos \frac{j\pi y}{L_y}$$

The dots represent the Observations.



Linear Algebraic Equations for the Coefficients a_{ij}

$$f(x_1^{ob}, y_1^{ob}) = \sum_i \sum_j b_{ij} \cos \frac{i\pi x_1^{ob}}{L_x} \cos \frac{j\pi y_1^{ob}}{L_y}$$

$$f(x_2^{ob}, y_2^{ob}) = \sum_i \sum_j b_{ij} \cos \frac{i\pi x_2^{ob}}{L_x} \cos \frac{j\pi y_2^{ob}}{L_y}$$

.....

$$f(x_M^{ob}, y_M^{ob}) = \sum_i \sum_j b_{ij} \cos \frac{i\pi x_M^{ob}}{L_x} \cos \frac{j\pi y_M^{ob}}{L_y}$$

Known b_{ij} → Analyzed Field

$$f(x,y) = \sum_i \sum_j b_{ij} \cos \frac{i\pi x}{L_x} \cos \frac{j\pi y}{L_y}$$

For General Ocean Basin → Generalized Fourier Series Expansion

Spectral Representation
Fourier Series Expansion

$$c(\mathbf{x}, z_k, t) = A_0(z_k, t) + \sum_{m=1}^{M} A_m(z_k, t)\ \Psi_m(\mathbf{x}, z_k),$$

Ψ_m → Basis functions (not sinusoidal)

c → any ocean variable

Determination of Basis Functions

- (1) Eigen Functions of the Laplace Operator (Data and Model Independent)
- (2) Empirical Orthogonal Functions (Data or Model Dependent)

Eigen Functions of Laplace Operator → Basis Functions (Closed Basin)

$$\triangle \Psi_k = -\lambda_k \Psi_k, \quad \Psi_k|_\Gamma = 0, \qquad k = 1, \ldots, \infty$$

$$\triangle \Phi_m = -\mu_m \Phi_m, \quad \frac{\partial \Phi_m}{\partial n}|_\Gamma = 0, \qquad m = 1, \ldots, \infty.$$

Ψ_k → Streamfunction

Φ_m → T, S, Velocity Potential

Basis Functions
(Open Boundaries)

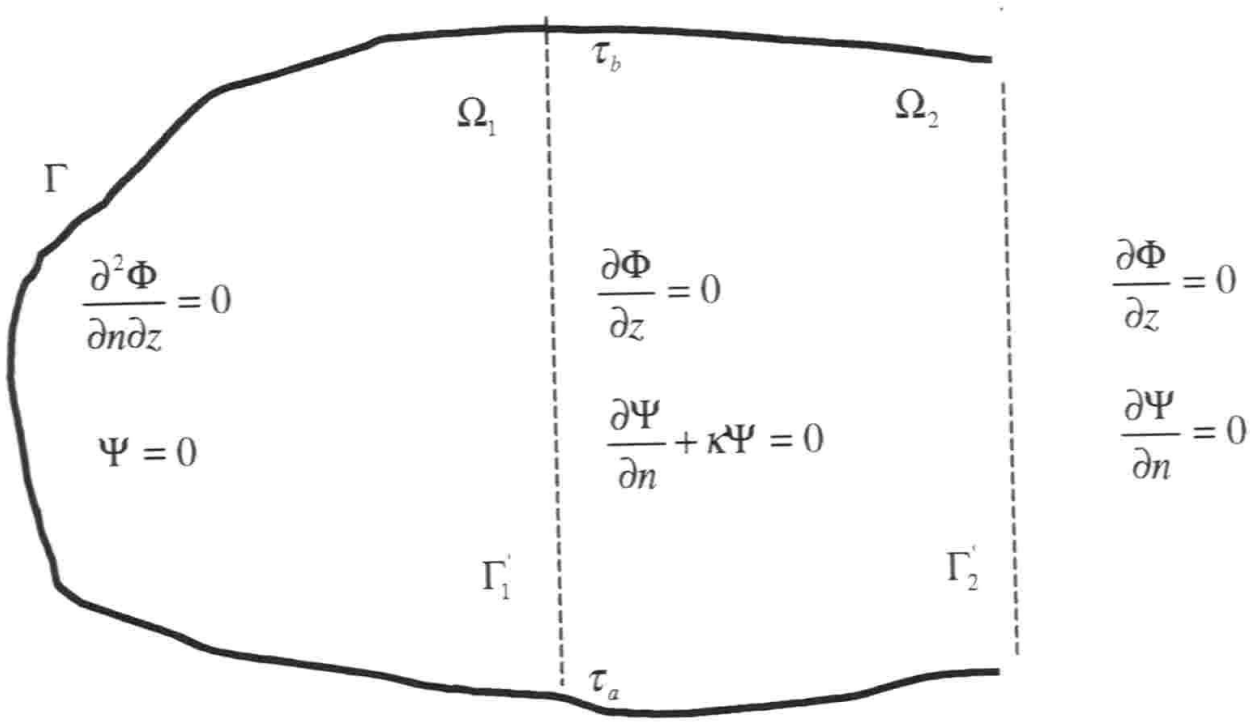
$$\triangle \Psi_k = -\lambda_k \Psi_k,$$

$$\triangle \Phi_m = -\mu_m \Phi_m,$$

$$\Psi_k|_\Gamma = 0, \quad \frac{\partial \Phi_m}{\partial n}|_\Gamma = 0,$$

$$\left[\frac{\partial \Psi_k}{\partial n} + \kappa(\tau)\Psi_k\right]|_{\Gamma_1'} = 0, \quad \Phi_m|_{\Gamma_1'} = 0,$$

Boundary Conditions



Spectral Decomposition

$$u_{KM} = \sum_{k=1}^{K} a_k(z,t^\circ)\frac{\partial \Psi_k(x,y,z,\kappa^\circ)}{\partial y} + \sum_{m=1}^{M} b_m(z,t^\circ)\frac{\partial \Phi_m(x,y,z)}{\partial x},$$

$$v_{KM} = -\sum_{k=1}^{K} a_k(z,t^\circ)\frac{\partial \Psi_k(x,y,z,\kappa^\circ)}{\partial x} + \sum_{m=1}^{M} b_m(z,t^\circ)\frac{\partial \Phi_m(x,y,z)}{\partial y}$$

$$T(\mathbf{x},t) = T_0(\mathbf{x}) + \sum_{m=1}^{M} c_m(t)\Phi_m(\mathbf{x})$$

$$S(\mathbf{x},t) = S_0(\mathbf{x}) + \sum_{m=1}^{M} d_m(t)\Phi_m(\mathbf{x})$$

Benefits of Using OSD

- (1) Don’t need first guess field
- (2) Don’t need autocorrelation functions
- (3) Don’t require high signal-to-noise ratio
- (4) Basis functions are pre-determined before the data analysis. They are independent on the data.

Optimal Mode Truncation

$$J(a_{1,\dots,}a_K, b_{1,\dots,}b_M, \kappa, P) = \frac{1}{2}\left(\left\|u_p^{obs} - u_{KM}\right\|_P^2 + \left\|v_p^{obs} - v_{KM}\right\|_P^2\right) \to \min,$$

Vapnik (1983) Cost Function

$$J_{emp} = J(a_{1,\ldots,}a_K, b_{1,\ldots,}b_M, \kappa, P).$$

$$\text{Prob}\left\{ \sup_{K,M,S} |\langle J(K,M,S)\rangle - J_{emp}(K,M,S)| \geq \mu \right\} \leq g(P,\mu)$$

$$\lim_{P\to\infty} g(P,\mu) = 0$$

Optimal Truncation

- Gulf of Mexico, Monterey Bay, Louisiana-Texas Shelf, North Atlantic

- $K_{opt} = 40$, $M_{opt} = 30$

Determination of Spectral Coefficients (Ill-Posed Algebraic Equation)

$$\mathbf{A}\hat{\mathbf{a}} = \mathbf{QY},$$

This is caused by the features of the matrix **A**.

Rotation Method (Chu et al., 2004)

Well-Posed → $$\mathbf{SA}\,\hat{\mathbf{a}} = \mathbf{SQY},$$

The matrix S is determined by

$$J_1 = \|\mathbf{A}\|^2 - \frac{\|\mathbf{SQY}\|^2}{\|\mathbf{a}\|^2} \rightarrow \max,$$

Errors

$$\bar{T}(\mathbf{x}) = \overbrace{T_0 + \sum_{l=1}^{48} D_l \Phi_l(\mathbf{x})}^{\hat{T}} + T'(\mathbf{x})$$

$$\bar{\mathbf{u}}(\mathbf{x},t) = \overbrace{C\Psi_0 + \sum_{n=1}^{24} A_n \nabla \times \mathbf{k}\Psi_n(\mathbf{x})}^{\hat{\mathbf{u}}} + \tilde{\mathbf{u}}(\mathbf{x}) + \mathbf{u}'(\mathbf{x})$$

T’ , **u**’ → errors

Noise-to-Signal Ratio → Error Estimation

$$\eta\left(\boldsymbol{\alpha},\boldsymbol{\beta}\right)=\frac{\left\|\boldsymbol{\alpha}\right\|_{(P)}}{\left\|\boldsymbol{\beta}\right\|_{(P)}}$$

$$\eta(T',T-T')\sim 0.1$$

(3) Upper Ocean Heat Content

Upper Ocean (0-300 m) Heat Content

$$HC = \int_{-h}^{0} \rho c T dz$$

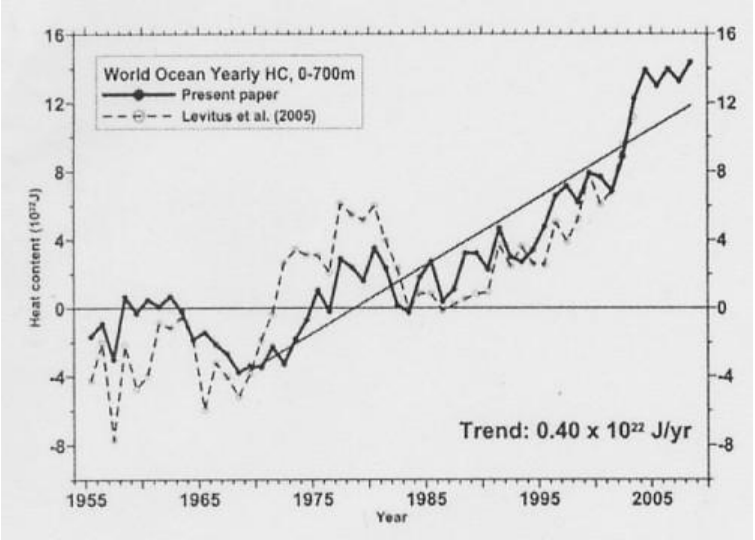
$HC = HC_{\text{mean}} + HC_{\text{seasonal}} + HC_{\text{anomaly}}$

EOF Analysis → HC_{anomaly}

→ Global Ocean Dipole Modes

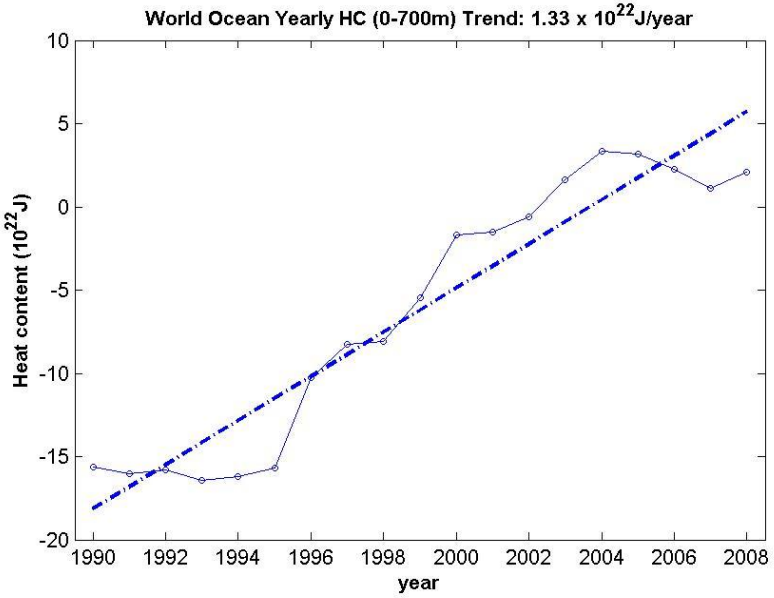
Trend of Upper Ocean (0-700 m) Heat Content

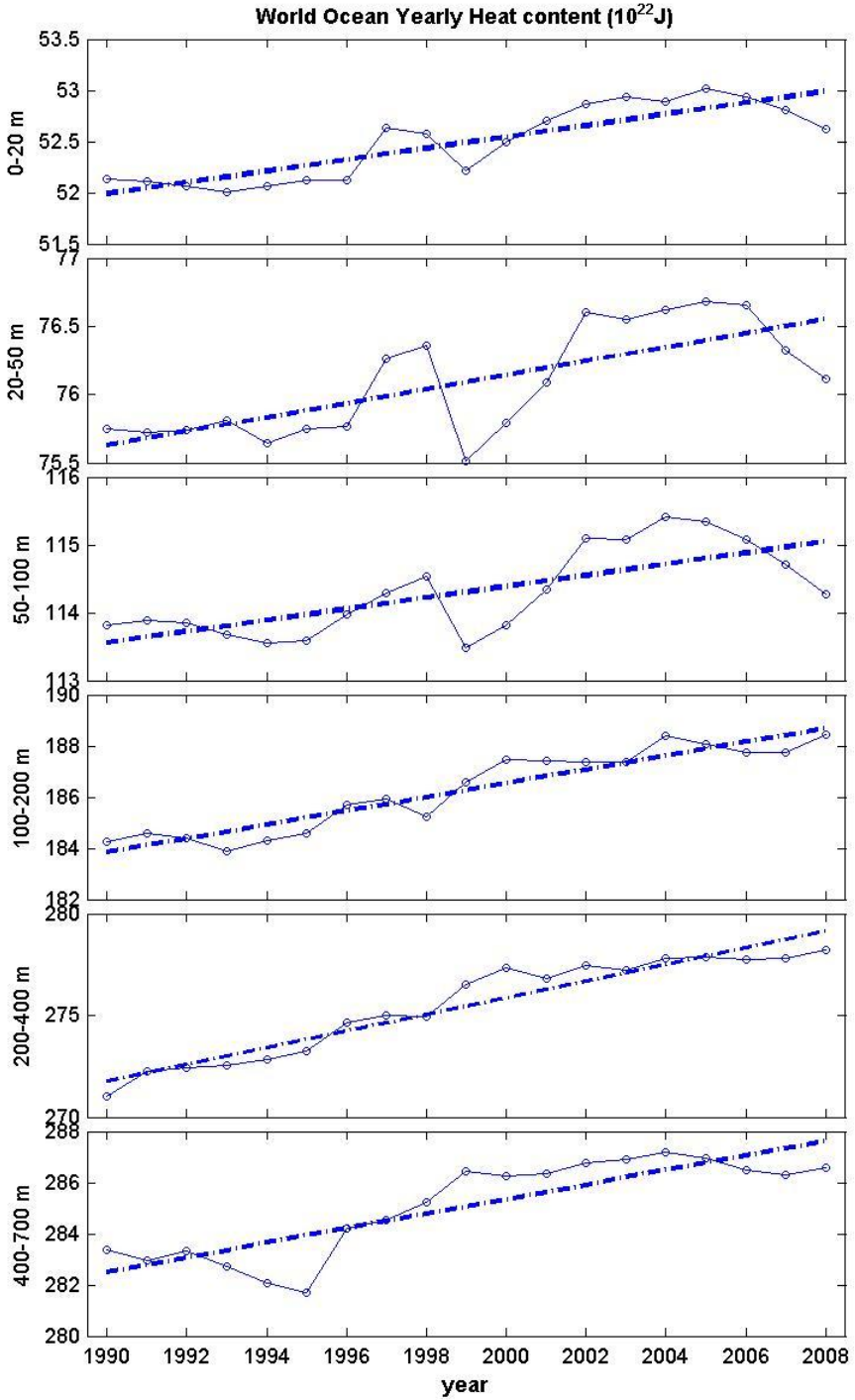
0.4 X 10^{22} J/yr
(1958-2008)
(Levitus et al.,GRL, 2009)
Without Argo data



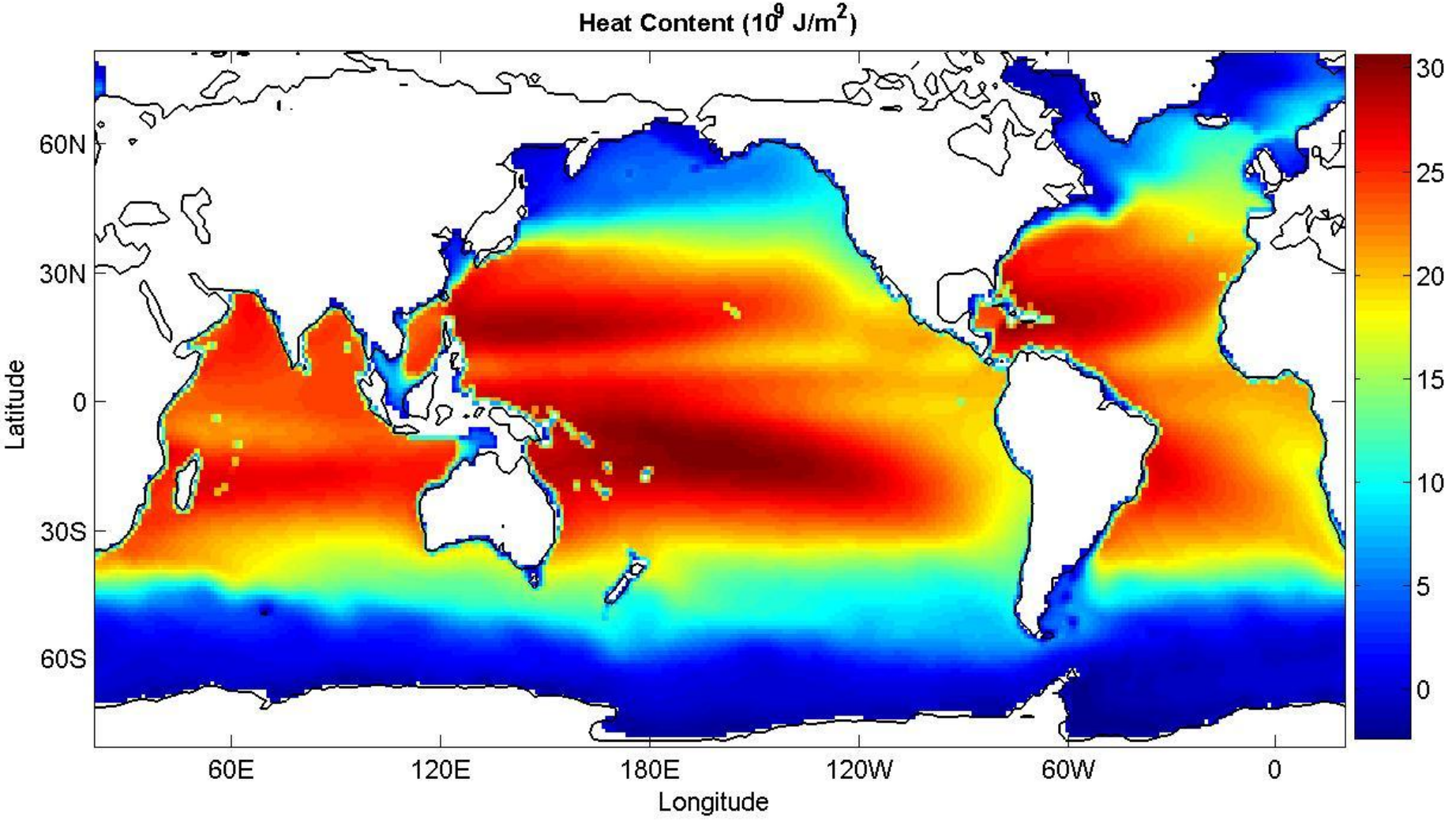
1.3 X 10^{22} J/yr
(1990-2008)

With Argo data



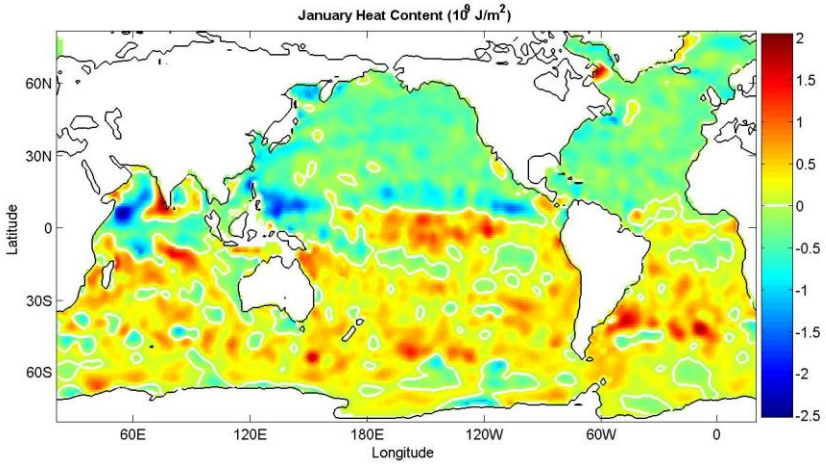

World Ocean Yearly Heat content (10^{22}J)
0-20 m
20-50 m
50-100 m
100-200 m
200-400 m
400-700 m
53.5
53
52.5
52
51.5
77
76.5
76
75.5
116
115
114
113
190
188
186
184
182
280
275
270
288
286
284
282
280
1990
1992
1994
1996
1998
2000
2002
2004
2006
2008
year

Upper Ocean (0-300 m) Mean Heat Content (J/m^2) (1990-2009)

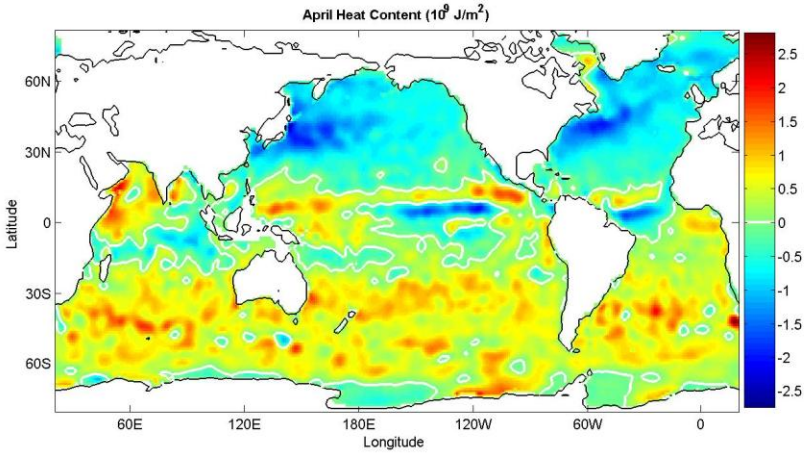


Seasonal Variability of Upper Ocean (0-300 m) Heat Content (J/m^2) (1990-2009)

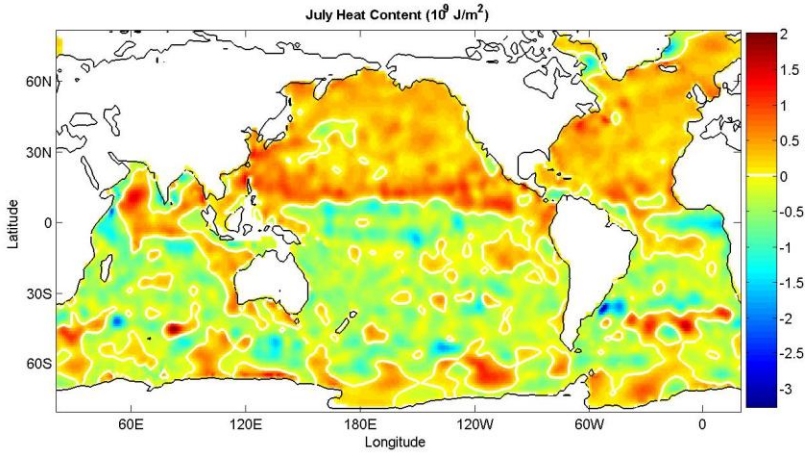
January



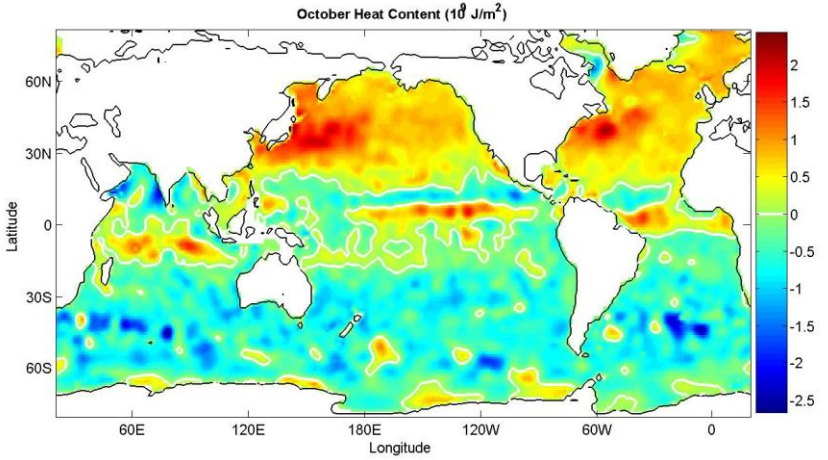
April



July



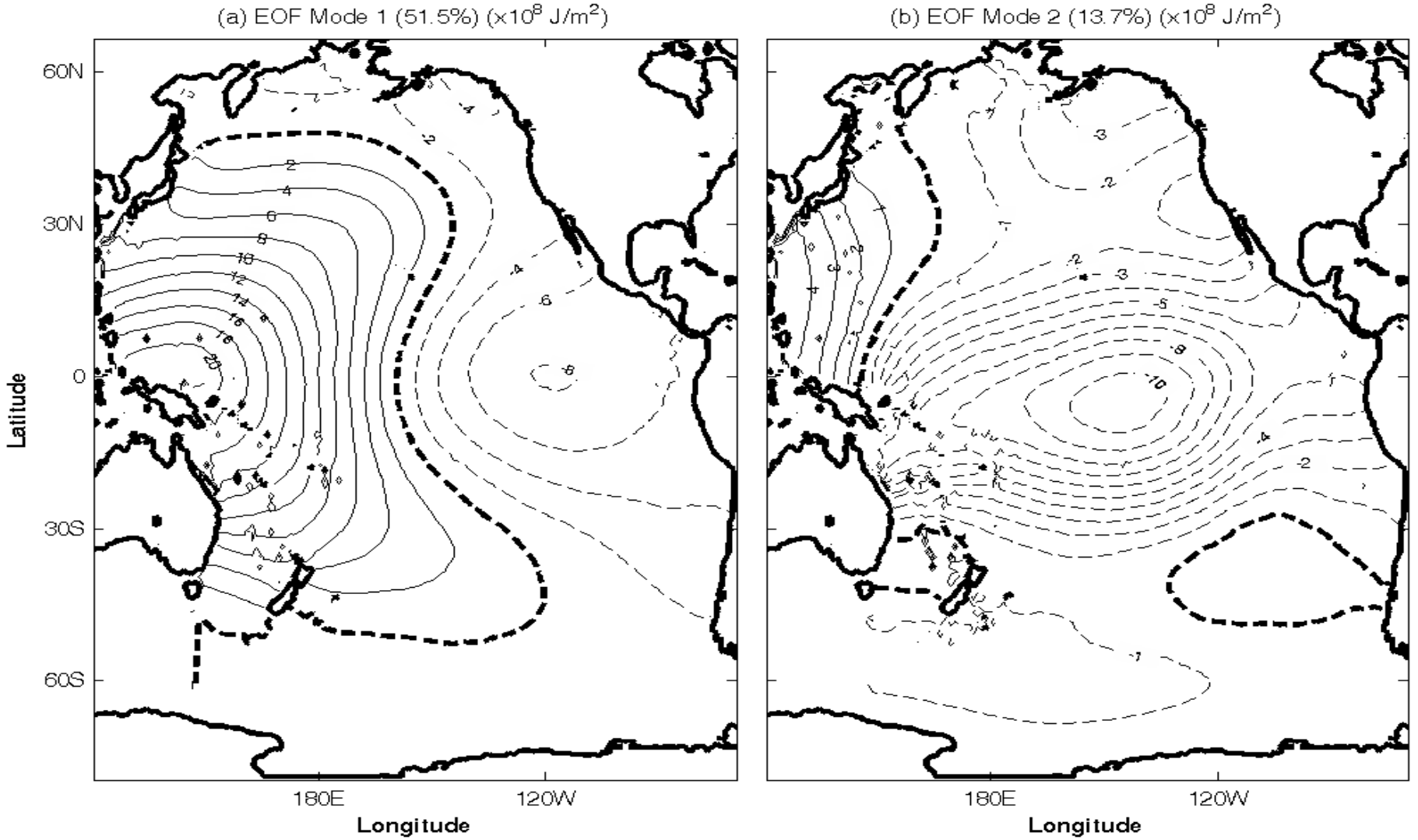
October



EOF Analysis →

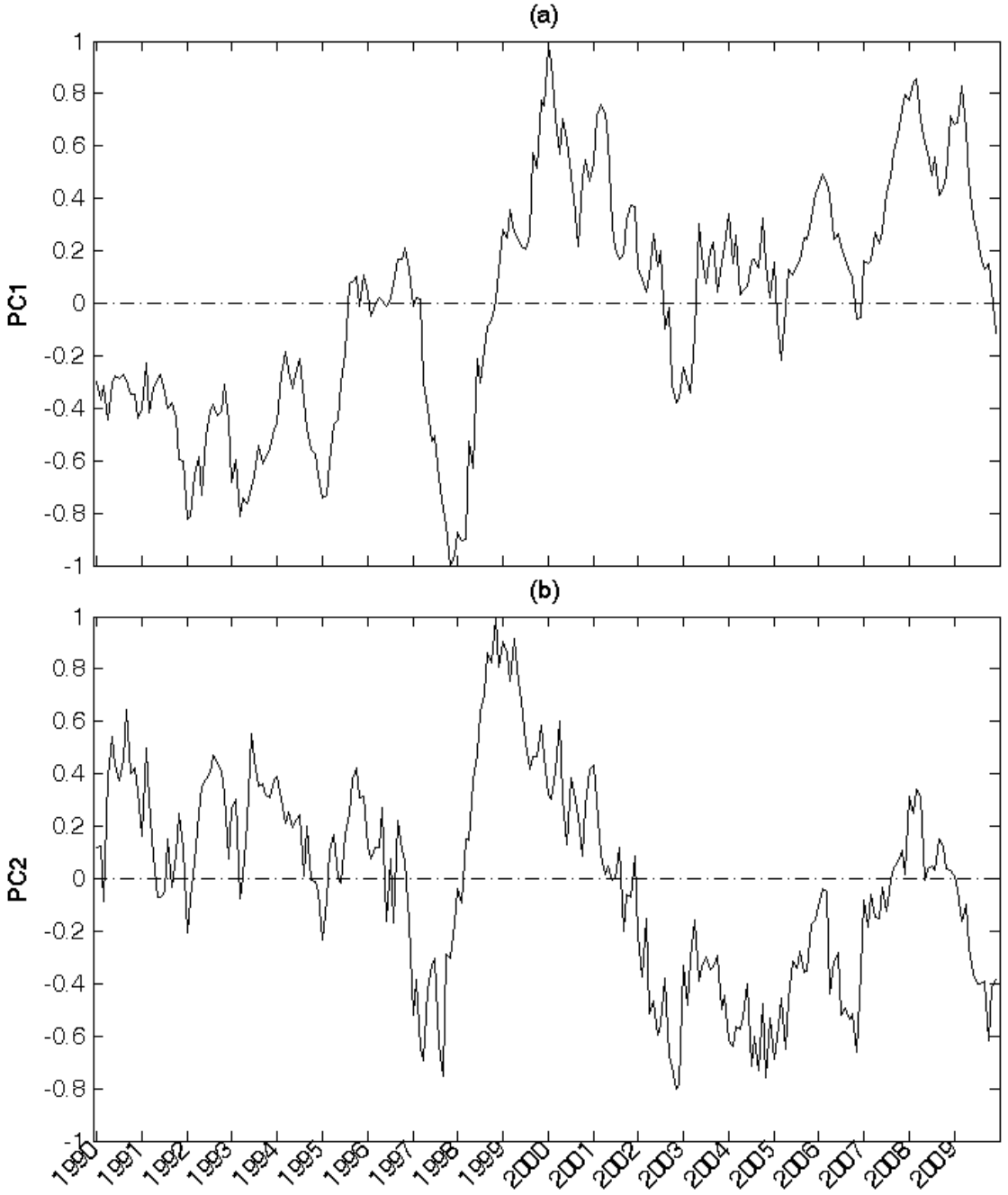
Heat Content Anomaly Relative to Seasonal Variation

EOF-1 (51.5%) → Canonical El Nino
EOF-2 (13.7%) → El Nino Modoki
Pacific Ocean (in 10^8 J/m^2)



PC1

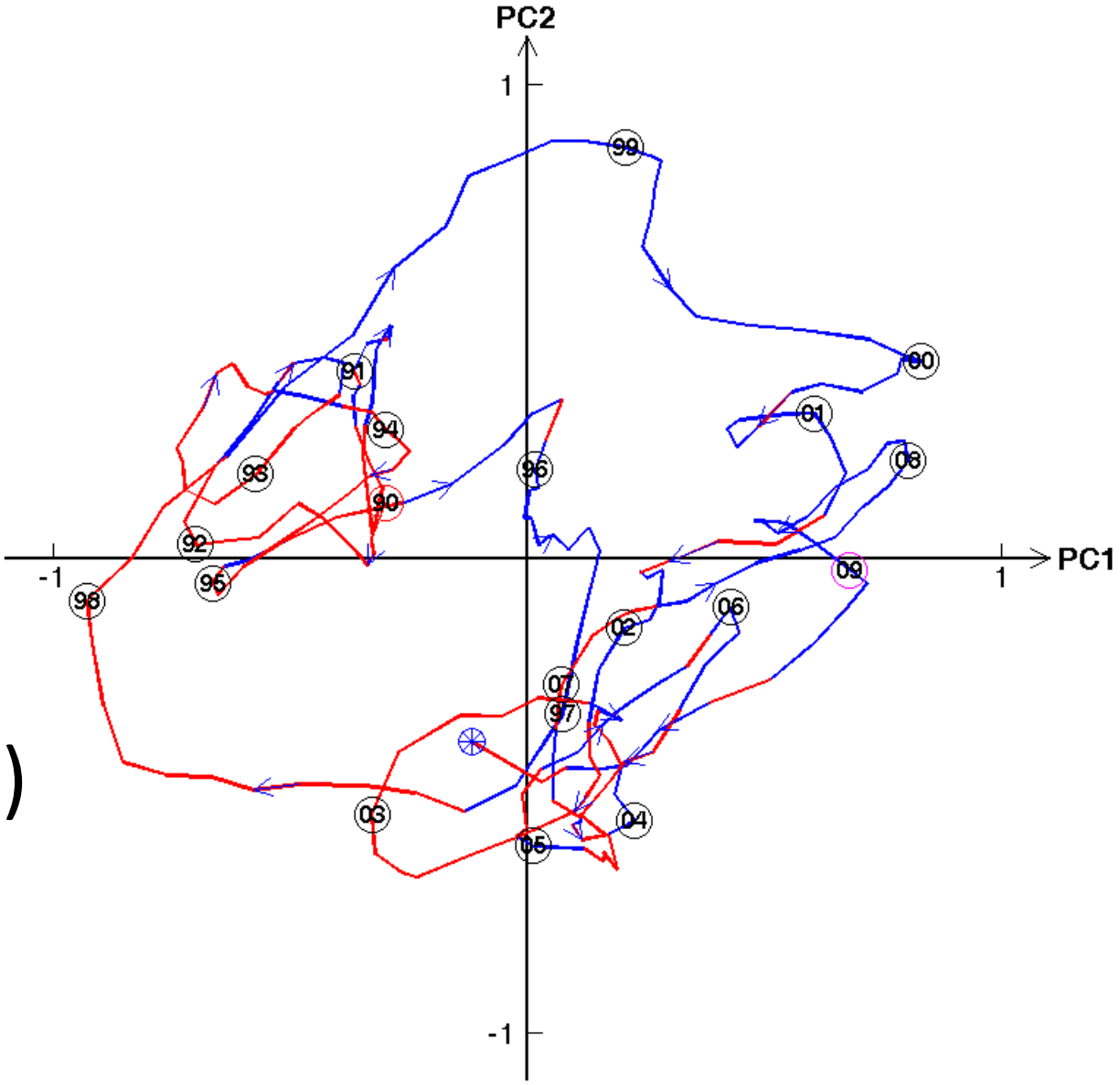
PC2


(a)
PC1
1
0.8
0.6
0.4
0.2
0
-0.2
-0.4
-0.6
-0.8
-1
(b)
PC2
1
0.8
0.6
0.4
0.2
0
-0.2
-0.4
-0.6
-0.8
-1
1990
1991
1992
1993
1994
1995
1996
1997
1998
1999
2000
2001
2002
2003
2004
2005
2006
2007
2008
2009

Phase Diagram (Pacific)

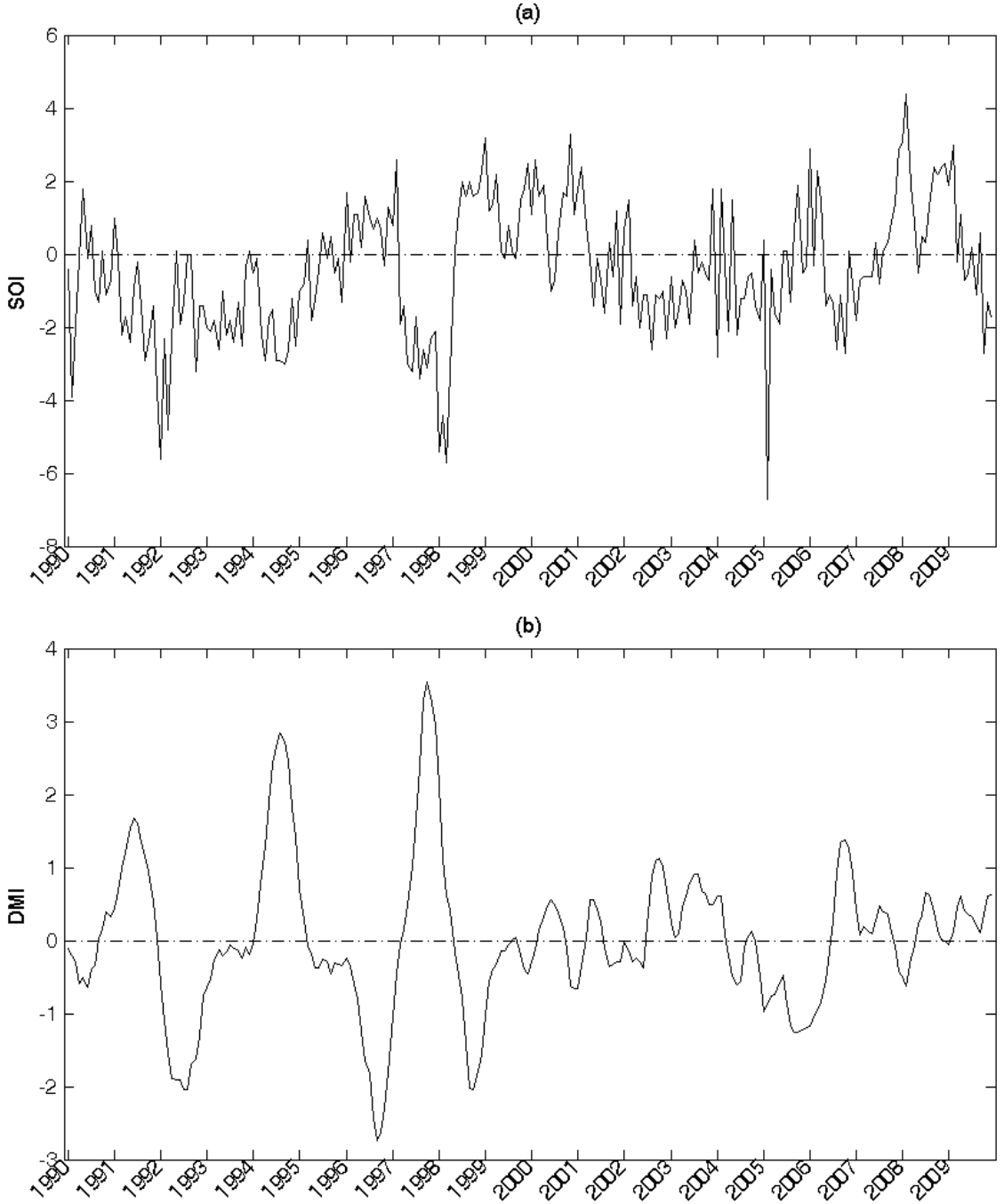
Red → SOI (-)

Blue → SOI (+)



Southern Oscillation Index (SOI)

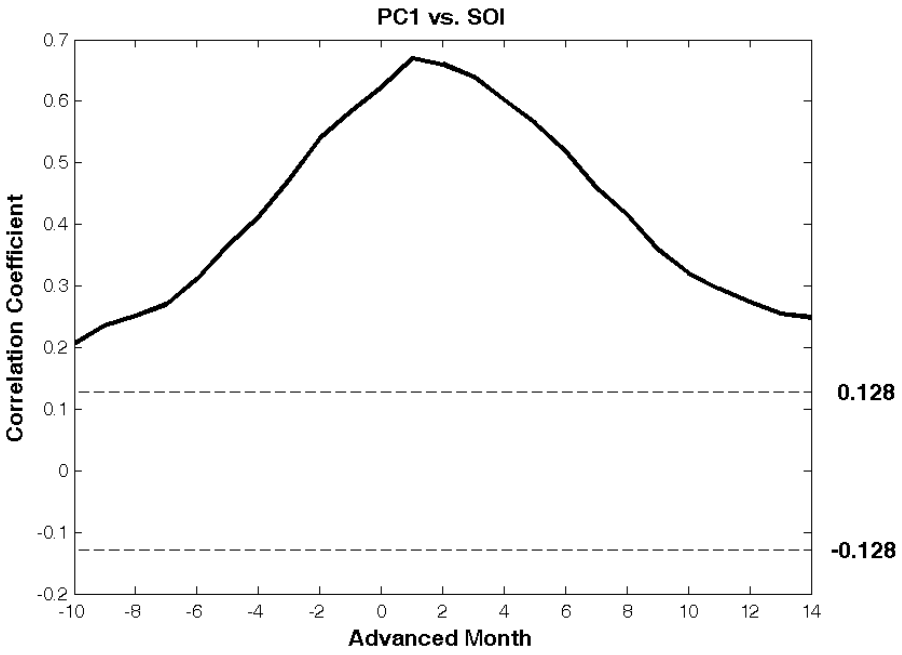
Dipole Mode Index (DMI)

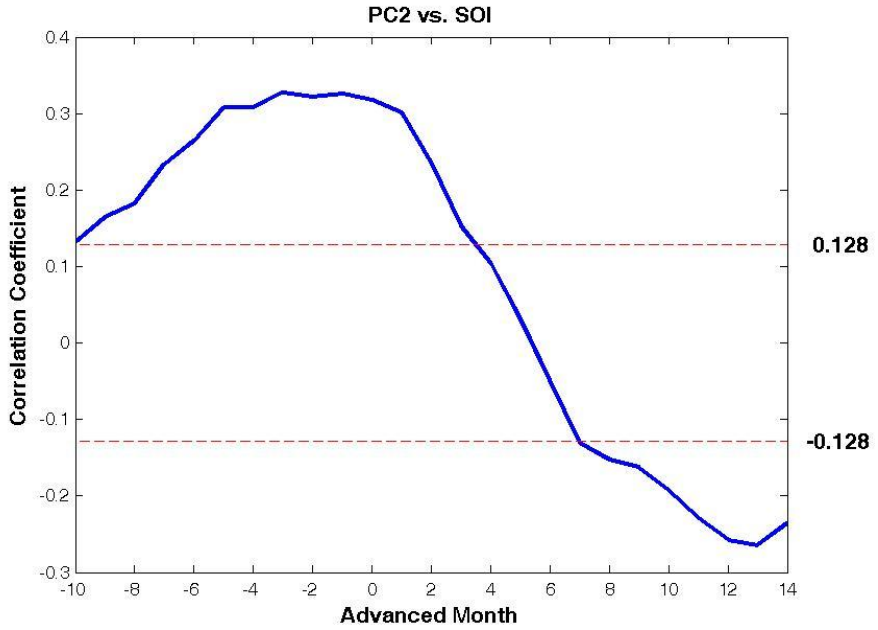


Lag-Correlation Coefficients

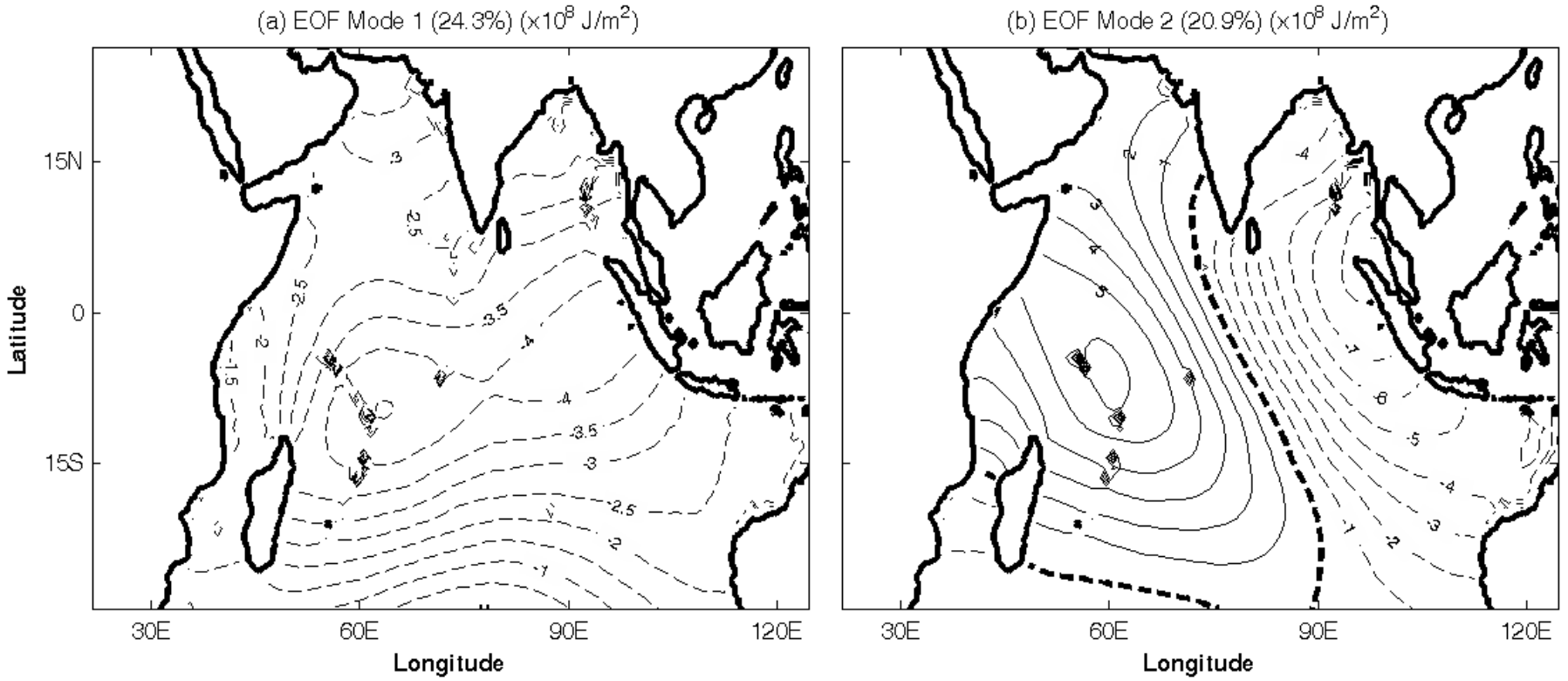
PC1 ←→ SOI

PC2 ←→ SOI





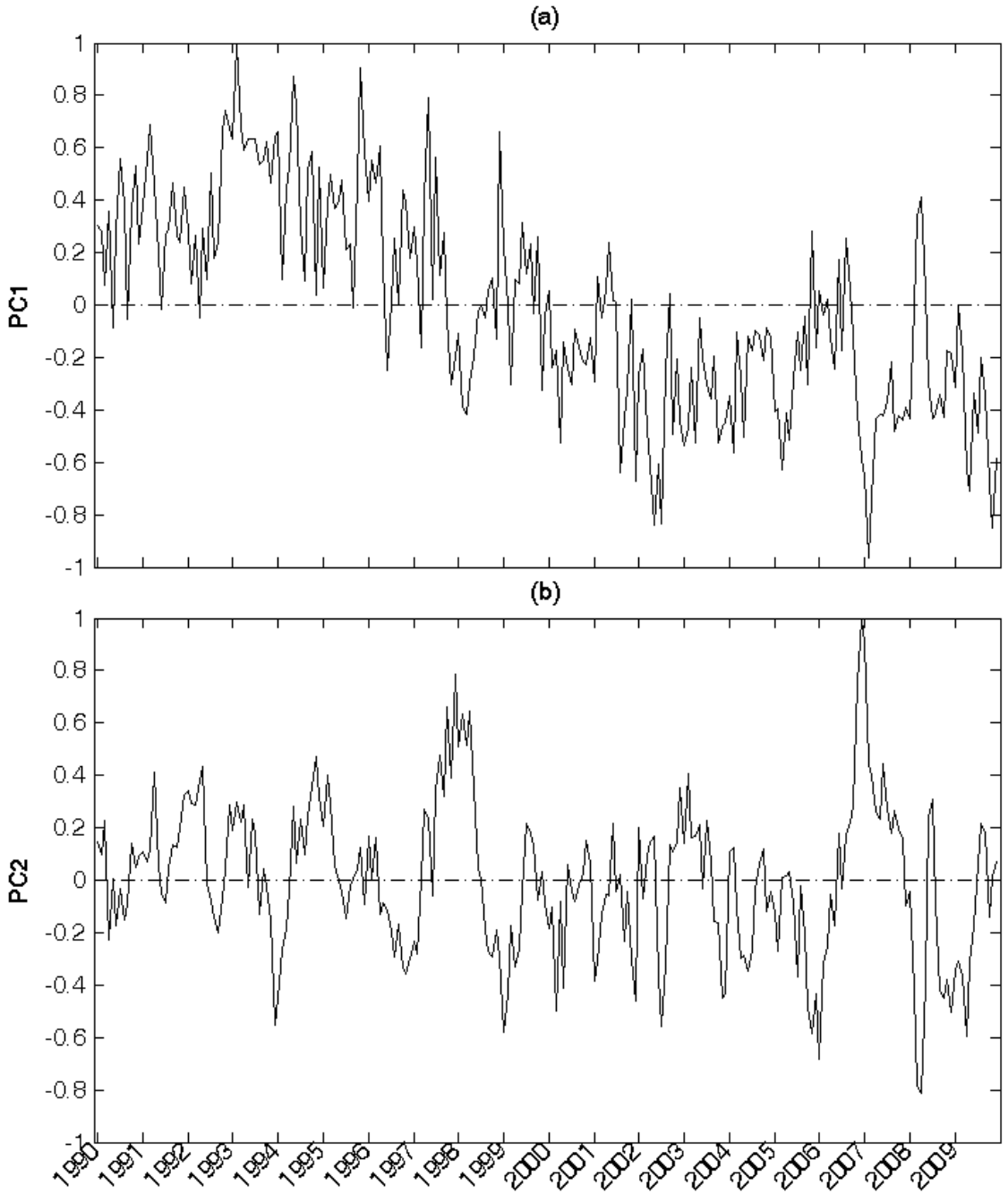
EOF-1 (24.3%) → Basin-scale Oscillation
EOF-2 (20.9%) → Dipole Mode
Indian Ocean (in 10^8 J/m^2)



PC1

→ Decadal

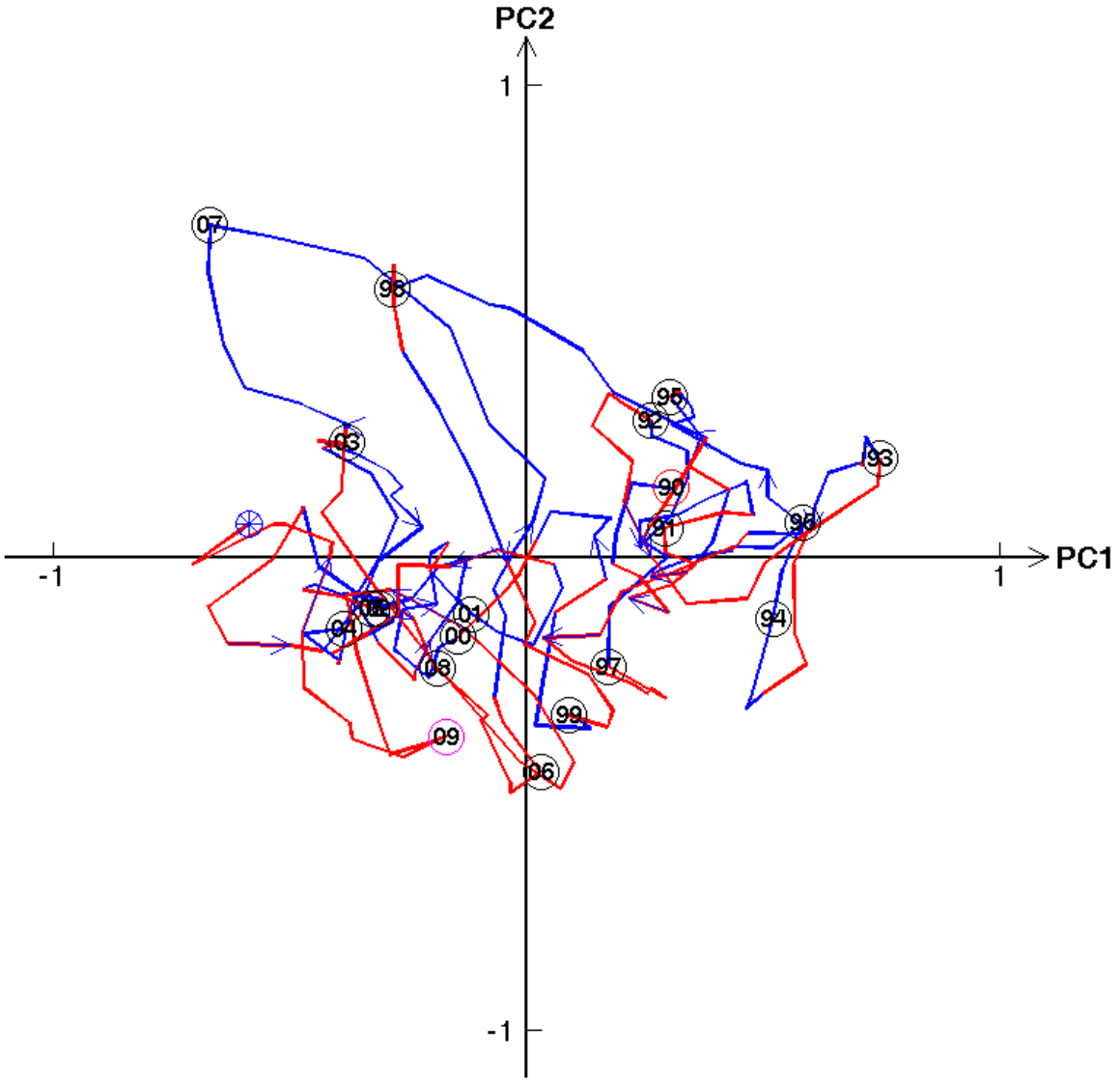
PC2



Phase Diagram (Indian)

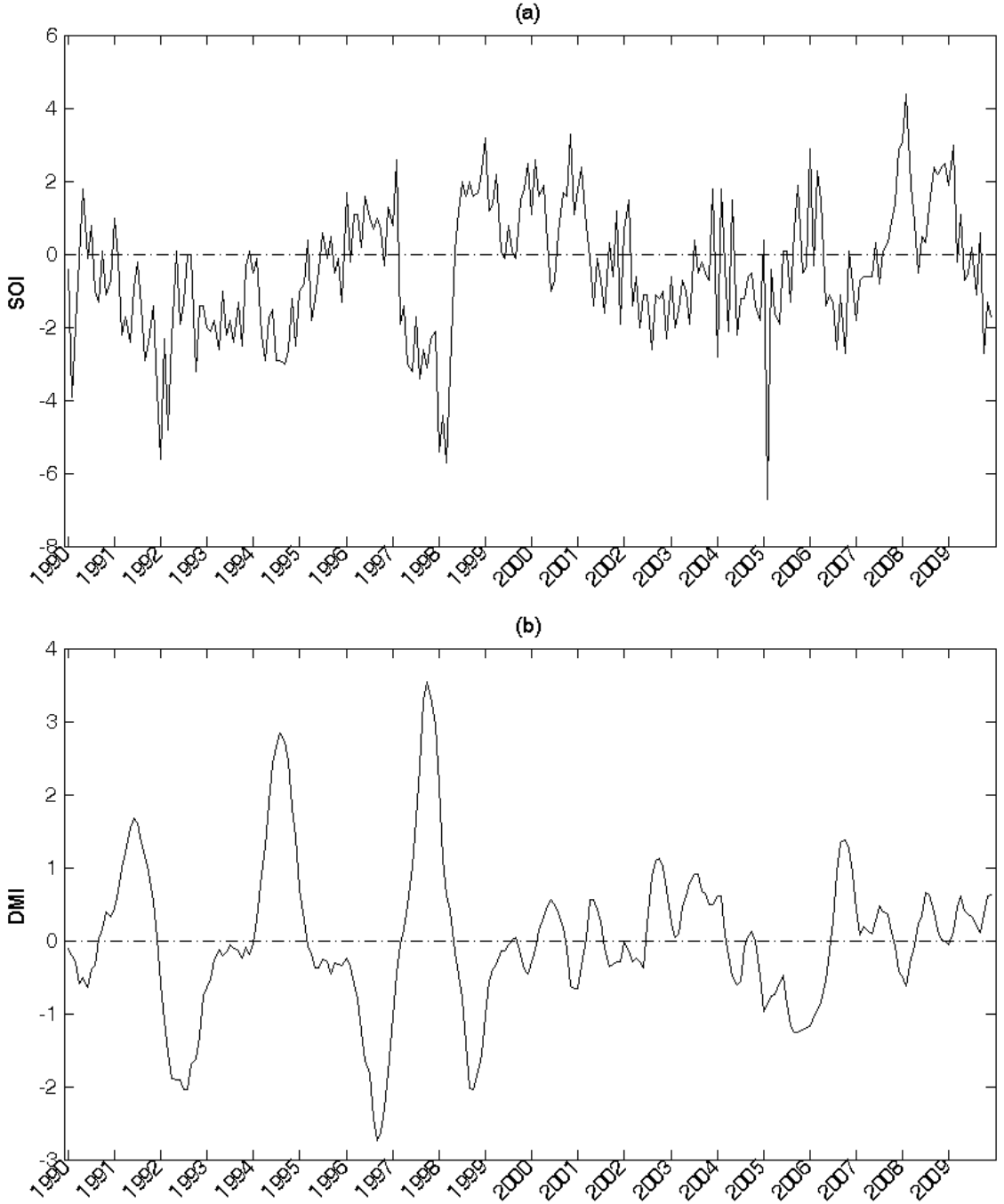
Red → DMI (-)

Blue → DMI (+)

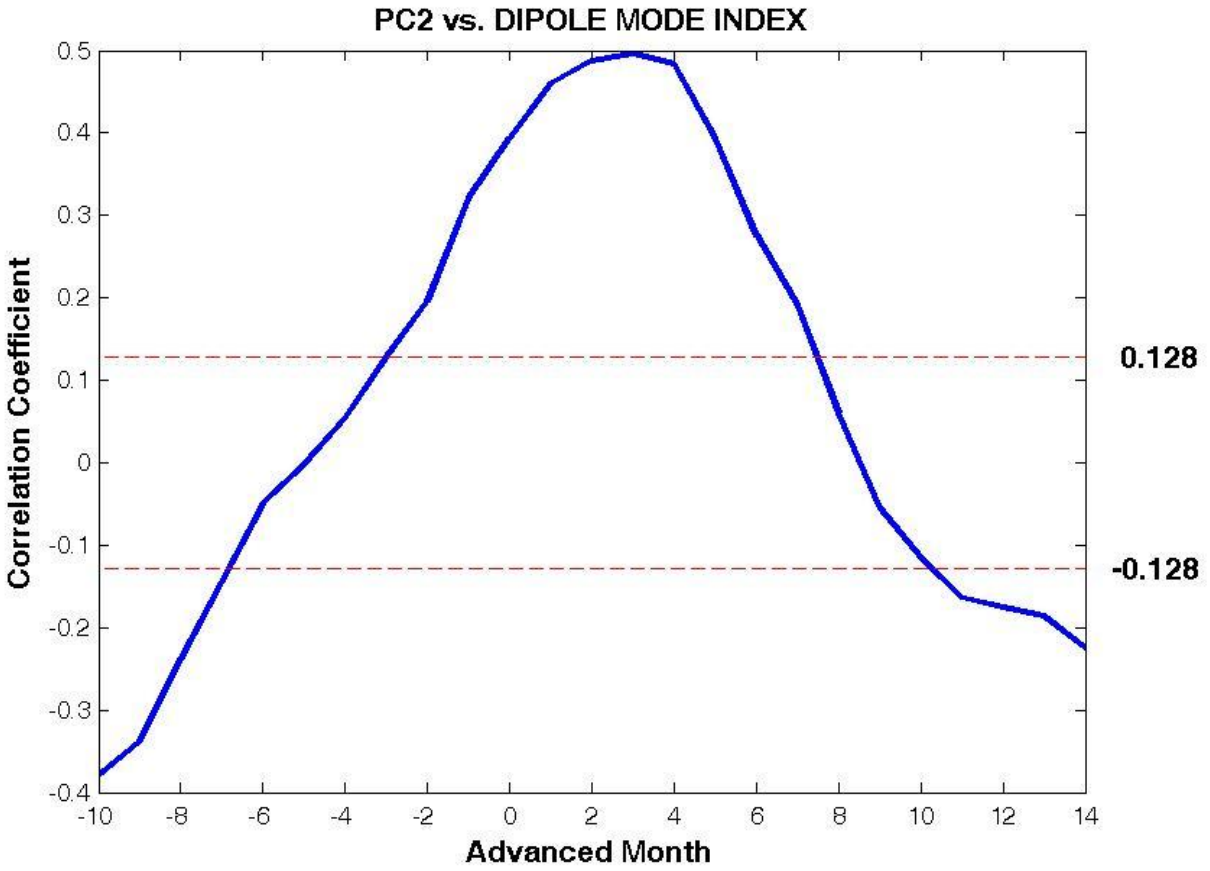


Southern Oscillation Index (SOI)

Dipole Mode Index (DMI)

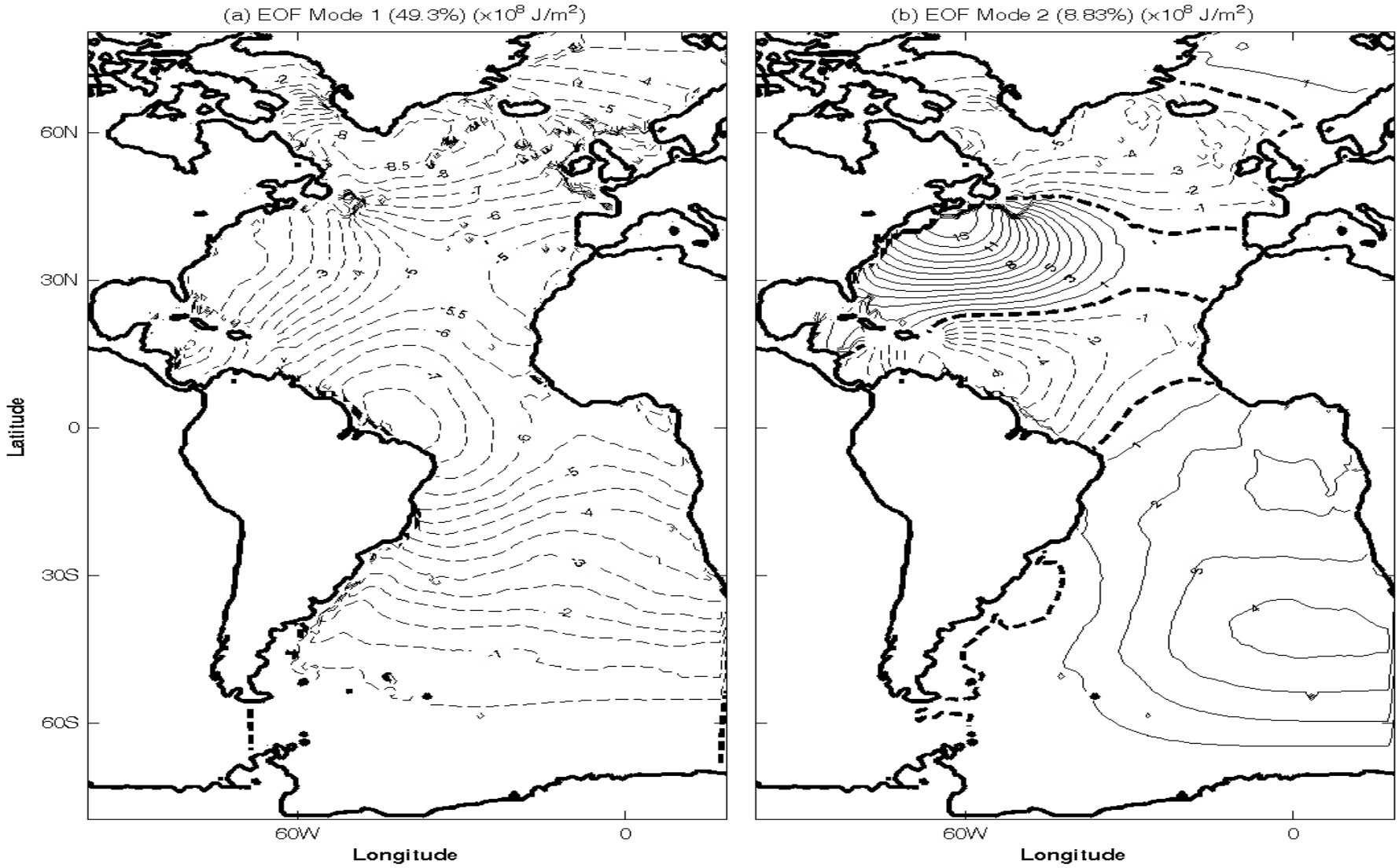


Lag Correlation between PC2 and DMI



Positive Month → PC2 advancing DMI

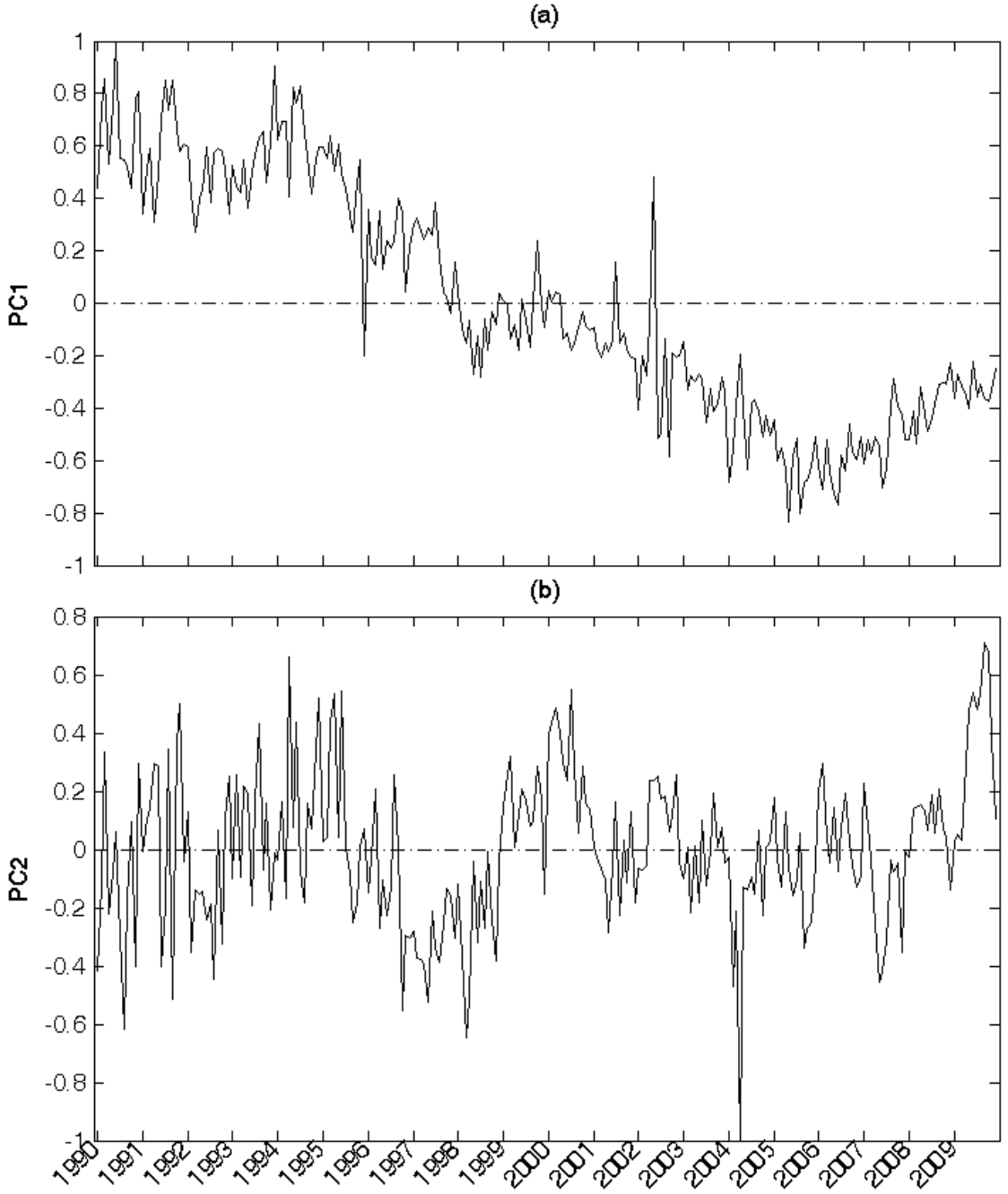
EOF-1 (49.3%) → Basin-Scale Oscillation
EOF-2 (8.8%) → Zonal Variability
Atlantic Ocean (in 10^8 J/m^2)



PC1

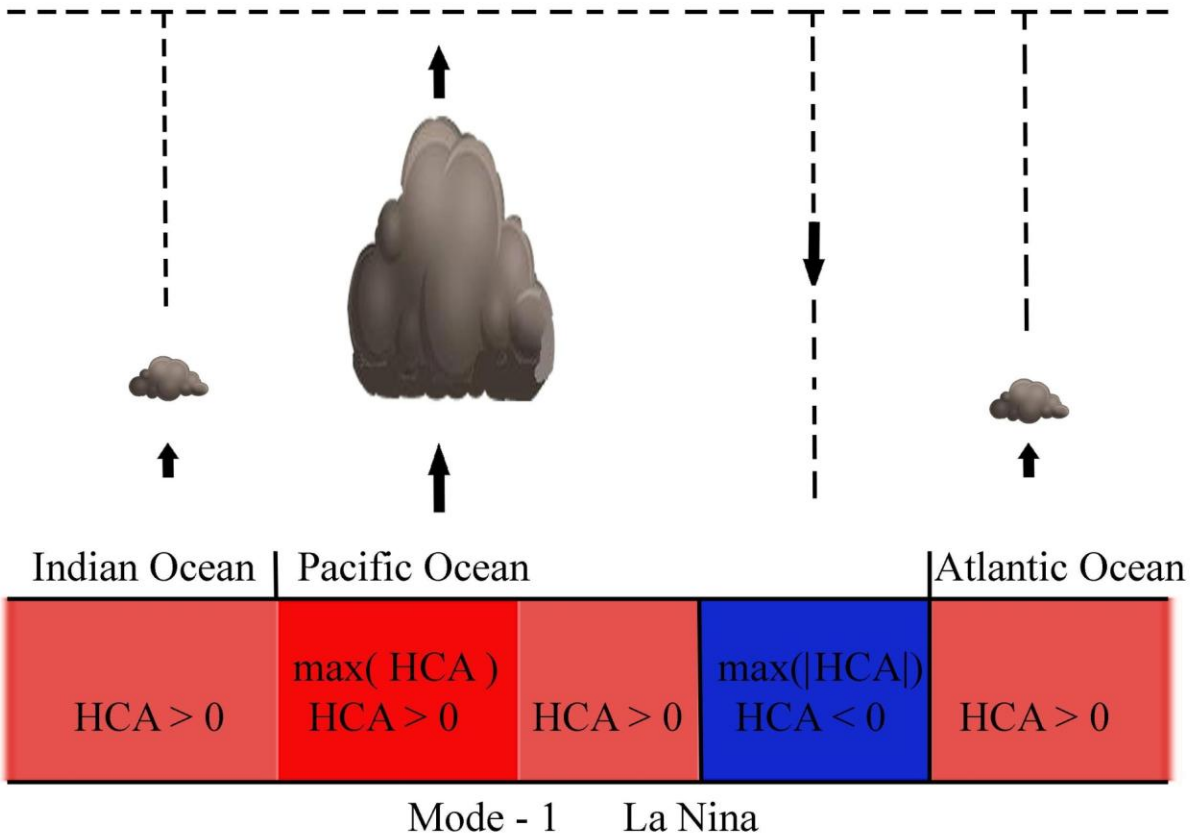
→ Decadal

PC2

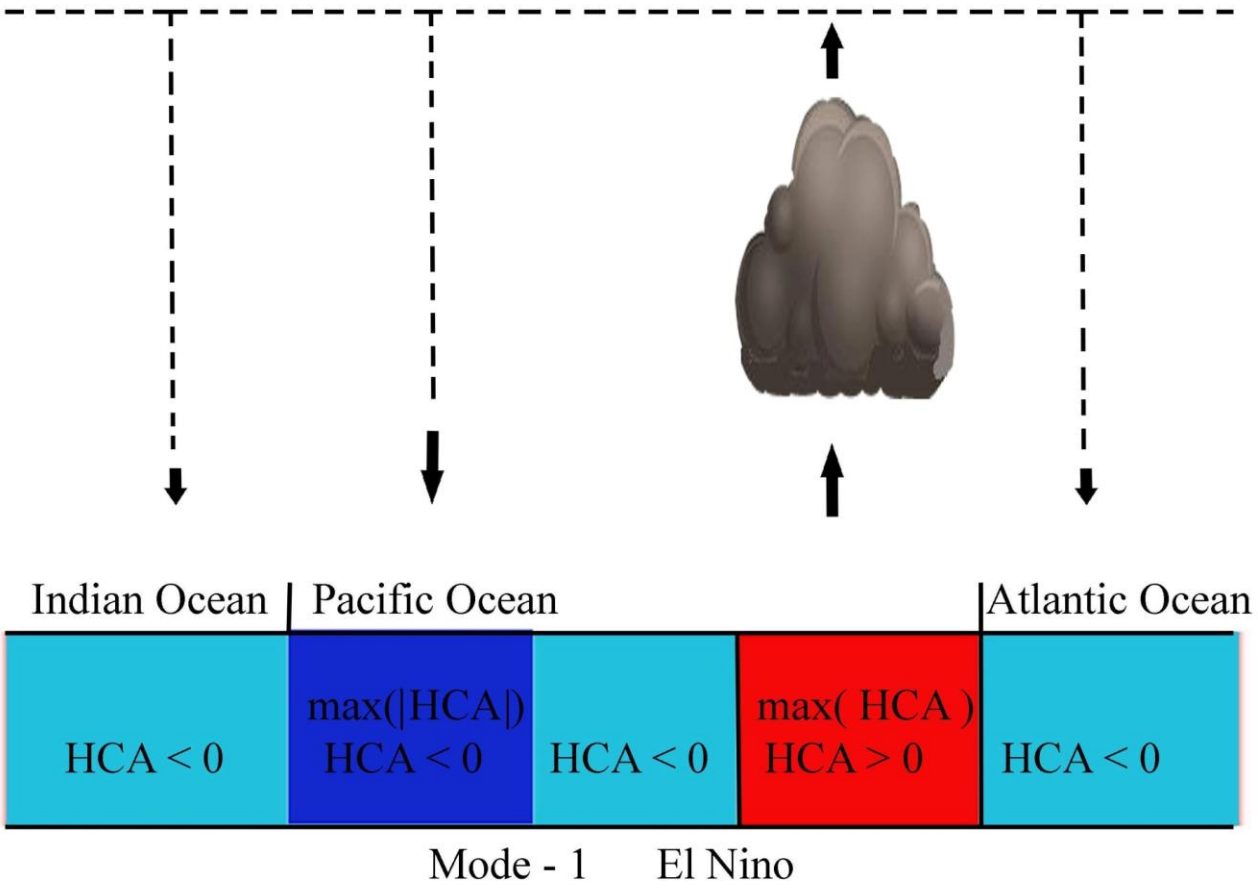


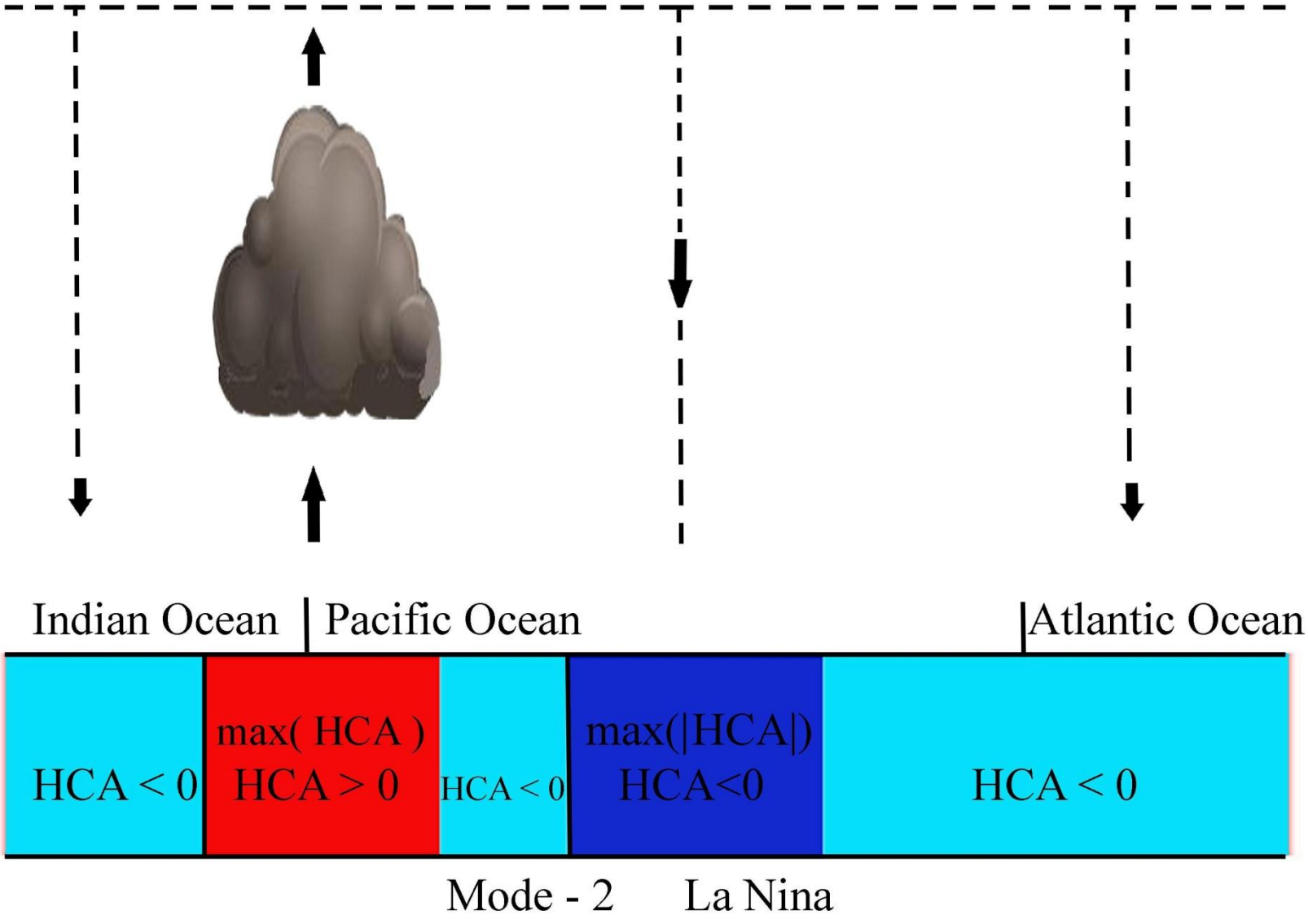
(4) Global Ocean Tripole

Canonical La Nina →
More and Stronger Hurricanes in Atlantic (Pielke and Landsea, 1999 BAMS)



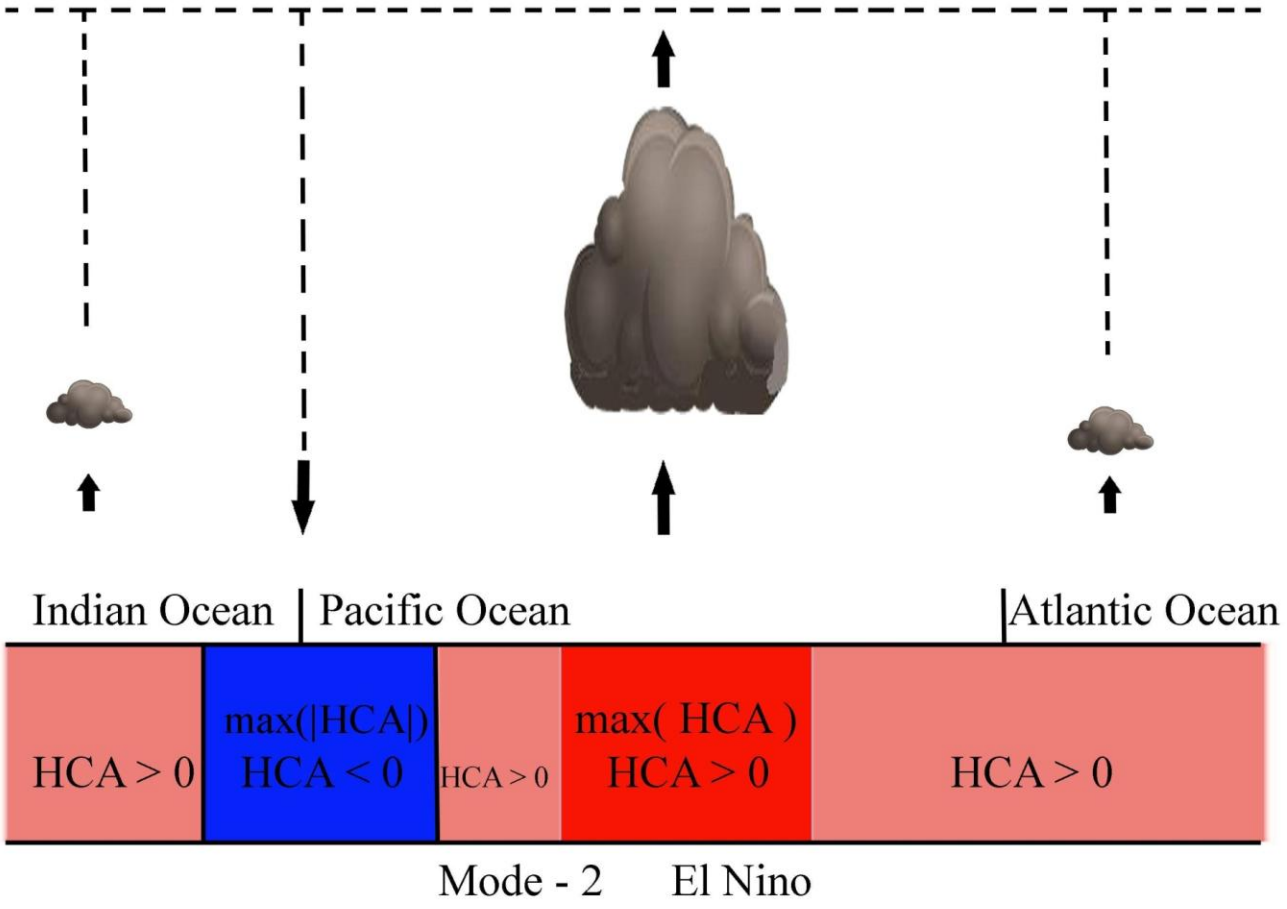
Canonical El Nino




Indian Ocean
Pacific Ocean
Atlantic Ocean
HCA < 0
max(HCA)
HCA > 0
HCA < 0
max(|HCA|)
HCA<0
HCA < 0
Mode - 2
La Nina

El Nino Modoki

More and Stronger Hurricanes in Atlantic



Conclusions

- (1) Upper ocean heat content contains the signal for climate change (interannual) → Global Ocean Tripole.

- (2) El Nino, El Nino Modoki, and Indian Ocean Dipole can be unified by Global Ocean Tripole.